Wave-impact driven dune face erosion processes

An analysis using stereo video observations and in-situ measurements

July 2007

Z4278.00

Wave-impact driven dune face erosion processes

An analysis using stereo video observations and in-situ measurements

M.Sc. Thesis Inge Kateman

Supervisors:
prof. dr. ir. M.J.F. Stive
dr. ir. A.J.H.M. Reniers
dr. ir. W.S.J. Uijttewaal
ir. A.B. Cohen
ir. J.S.M. van Thiel de Vries

July 2007

Preface

This M.Sc. thesis study forms the completion of my education at the Delft University of Technology in The Netherlands, faculty of Civil Engineering and Geosciences, Department of Hydraulic Engineering. This thesis study has been carried out at WL | Delft Hydraulics.

I would like to thank my supervising committee, prof. dr. ir. M.J.F. Stive (Delft University of Technology), dr. ir. A.J.H.M. Reniers (Delft University of Technology), dr. ir. W.S.J. Uijttewaal (Delft University of Technology), ir. A.B. Cohen (WL | Delft Hydraulics) and ir. J.S.M. van Thiel de Vries (Delft University of Technology, WL | Delft Hydraulics) for sharing their knowledge and for their help during the realisation of this thesis.

Furthermore I would like to thank Martijn Coeveld, Robin Morelissen, Ap van Dongeren, Jamie Lescinski, Joop van der Pot, Irv Elshoff, Wim Bakker, Marcia de Jongh and Erik van Velzen from WL | Delft Hydraulics for their contribution in any way to my research and report. Moreover I would like to thank the other graduate students at WL | Delft Hydraulics for an unforgettable period at the “Afstudeereiland”. Paula, Marieke, Robert-Jan, Pieter, Marjella, Claartje, Noud, Bas, Laura, Anton, Ali, Nathanael and Annelies, you were of immeasurable support during my complete graduation time.

Last but not least, I would like to thank all my friends and family who helped and supported me during the last few months to realise the research, report and presentation. Considering the past eight years, I am very grateful to everyone who contributed to the great memories of my entire student time in Delft.

Inge Kateman
Delft, June 2007

Contents

Appendices

List of Tables

List of Figures

List of Photographs

List of Symbols

Latin symbols

A	m^2	retreat area
c_g	m/s	wave celerity
D_{50}	m	grain size diameter such that 50 % of the grains by mass are smaller than D = D50
F	N/m^1	wave impact per meter width
f_s	Hz	frequency of slump events
g	m/s^2	gravitational acceleration
H_{m0}	m	significant wave height based on wave spectrum
h_{in}	m	water depth for incoming waves
h_{swi}	m	maximum wave height of a bore
h	m	instantaneous water depth
h_0	kg/m^3	water depth corresponding with still water level
n_p	-	porosity
P	m^3/m^1	primary erosion volume
p	$kgm/s/m^1$	momentum
Q_{in}	$m^3/s/m^1$	discharge per meter width for incoming waves
Q_{out}	$m^3/s/m^1$	discharge per meter width for outgoing waves
S	m^3/m^1	secondary erosion volume
SF	N/m^1	impact of an individual wave per meter width
SVE	m^3/m^1	specific erosion volume
s_p	-	wave steepness at deep water based on peak wave period
$s_{m-1,0}$	-	wave steepness at deep water based on spectral wave period
ΔT	s	period of time during which wave impacts take place
$T_{m-1,0}$	s	spectral wave period
T_p	s	peak wave period, defined as the period in an arbitrary wave spectrum with a global maximum of the spectral density
Δt	s	time step of in-situ measurements
t_1	s	start of the period of time during which wave impacts take place
t_1	s	end of the period of time during which wave impacts take place
u	m/s	flow velocity
u_{swi}	m/s	leading edge velocity of a bore
u_{in}	m/s	flow velocity for incoming waves
u_{out}	m/s	flow velocity for outgoing waves
V_{tot}	m^3/m^1	total erosion volume as derived from average in-situ measured profiles
V_1	m^3/m^1	dune erosion volume above still water level as derived from average in-situ measured profiles
V	m^3	volume
V_V	m^3	individual slump erosion volume directly derived from video
V_A	m^3	individual slump erosion volume derived from retreat areas
x	m	horizontal distance in along-flume direction
y	m	horizontal distance in cross-flume direction
z	m	vertical distance

Greek symbols

Δ	-	difference
η	m	surface elevation
η_{in}	m	surface elevation for incoming waves
η_{out}	m	surface elevation SWL for outgoing waves
φ	°	camera Azimuth
ρ	kg/m^3	mass density of water
ρ_s	kg/m^3	mass density of sand
σ	°	camera roll
τ	°	camera tilt

1 Introduction

1.1 Background

Sandy coasts are often subject to shoreline retreat. Shoreline retreat is on the one hand a socio-economic issue, as valuable area might get lost on the long term. On the other hand, when dune ridges serve as the primary water defence, shoreline retreat implies dune erosion and therefore the safety of the hinterland is jeopardised.

Dune erosion mainly occurs under storm conditions, when the water level and waves are relatively high and waves directly hit the dune face. Sediment eroded from the dune face during a storm is added to the active swash system in front of the dune and is redistributed over the beach and foreshore. In the period following the storm, this sediment is gradually relocated again, its direction depending on the occurring hydraulic conditions in the surf and swash zone. In the absence of longshore transport gradients it is returned to its former location on the dune, therewith recovering the former dune profile. When a positive longshore transport gradient is present the sediment is transported in longshore direction. The dune profile will then never recover, implying shoreline retreat.

For socio-economic and safety reasons it is desirable to be able to model shoreline retreat. Thorough understanding of dune erosion and swash zone processes and interaction between the two is therefore required. Swash zone and inner surf sediment transport needs to be accurately modelled to predict cross-shore profile changes. A sub model that describes dune face erosion as a result of hydraulic forcing is an essential part of predicting sediment transport in the swash zone. For the modelling of dune face erosion, several approaches have been proposed. Some of these are process-based, which implies that the model predicts sediment fluxes on the dune and in the swash zone and therewith predicts the response of the dune.

One process-based approach by Fisher *et al.* (1986) relates an individual wave impact on the dune face to the instantly resulting dune face erosion volume. In their dune erosion model the total erosion of a dune during a storm is considered as the summation of the specific erosion volumes from single impacts on the dune face. A linear relation was found between specific wave force and specific dune erosion volume. This reveals a dependency of dune erosion volumes on wave impacts. This model does however not directly predict erosion volume per unit of time. Sediment fluxes can only be modelled when the specific wave impacts are combined with the specific wave periods.

Observations during storms in the field or during dune erosion experiments in flumes reveal that a typical periodical phenomenon occurs when dunes erode. The dune face gradually steepens under continuous wave attack until a volume of sand comes loose. This volume then slides down the dune face and falls apart on the beach in front of the dune face.

1.2 Problem description

The occurrence of periodical slump events is a crucial phenomenon in the erosion process. This finding has the following consequences for the development of a wave-impact driven dune face erosion model:

- The frequency and magnitude of slump events together determine sediment flux.
- As multiple waves are necessary to induce a slump event, wave impact is among others determined by the period during which waves attack the dune face.

The current wave-impact driven dune face erosion model by Fisher *et al.* (1986) does not account for these influences on the relation between wave impact and sediment flux from the dune face.

1.3 Objective

The objective of this research is to study the relation between wave impact and sediment flux from the dune face using an approach based on the one previously proposed by Fisher *et al.* (1986), but taking into account the phenomenon of slump events.

1.4 Approach

To asses the above hypotheses measurements of large-scale dune erosion experiments in the Delta flume, a research facility of WL | Delft Hydraulics, are analysed. First, a definition is described for wave impact and sediment flux. This is done based on the model by Fisher *et al.* (1986), but adapting the definitions by taking into account the periodicity of slump events.

To calculate wave impact and sediment flux several datasets are available of the Delta flume experiments. These are profiles derived from traditional in-situ profile measurements, in-situ pressure and flow velocity measurements and video data. The method or deriving values for wave impact and sediment flux is based on the specific definitions of these parameters.

Finally, the results of the calculations are analysed to establish whether the hypotheses can be either accepted or rejected.

1.5 Outline

Chapter 2 explains some relevant theory on dune erosion physics. Shoreline retreat is treated in general and the considered dune face erosion mechanisms in more detail. Chapter 3 elaborates on the data that will be used for this research. The physical model setup, test program and measurements of the large-scale Delta flume dune erosion experiments are explained, as well as relevant findings in the test results. In Chapter 4, the approach to dune erosion modelling used in this research is explained in more detail. First, different approaches on dune erosion modelling from previous studies are described. The approach by

Fisher *et al.* (1986) is elaborated on specifically. The altered definitions used for the purpose of this research are particularly explained. Chapter 5 presents and discusses the results when the adapted model is applied to the data of the Delta flume experiments. The findings from these results are discussed in Chapter 6. Chapter 7 presents the conclusions and recommendations that arise from this study.

2 Dune erosion physics

This chapter elaborates on dune erosion physics to clearly define what type of erosion is studied and to understand the physical processes concerned.

2.1 Shoreline retreat due to dune face erosion

Two types of erosion processes exist that affect dune and beach profiles of a sandy coast. These are erosion processes due to mean hydraulic conditions on the long term and erosion processes due to extreme hydraulic conditions such as storms or hurricanes on the short term. Generally, mean hydraulic conditions have effect on large time scales like years or seasons, while extreme events are particularly restricted to small time scales such as hours or days. An overview of the two causal relations is presented in Figure 2.1.

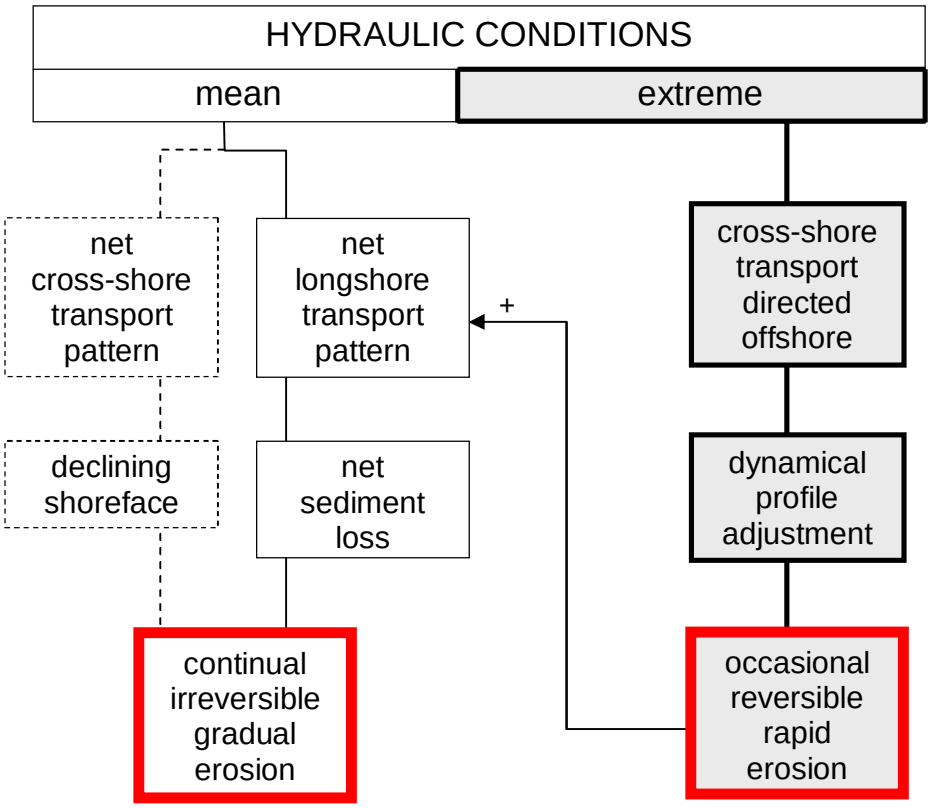

Figure 2.1 Overview of causal relations for beach and dune erosion (Steetzel, 1993). The occasional rapid erosion as a result of extreme events might lead to irreversible erosion when the mean conditions are such that there is a net longshore transport pattern. This is indicated with the arrow. Both occasional and gradual erosion might lead to decreased safety levels, indicated with the red rim. The focus of this research is on the short-term dune erosion processes during extreme conditions, which are marked as shaded blocks on the right side of the diagram.

Two long-term effects are illustrated on the left side of Figure 2.1. A combination of the two may also occur. In this research however, the focus will be on the short-term erosion processes, which have a different cause than long-term erosion. These short-term erosion

processes are marked by shaded blocks in the diagram of Figure 2.1. As short-term erosion may also have effect on the development of the shoreline on the long term, both short- and long-term erosion processes are shortly discussed here.

2.1.1 Long-term coastline development

On the long term, the development of a coastline is determined by the magnitude of the longshore transport gradient. This gradient may be originated by various factors, for example a longshore gradient in wave attack or currents occurring at non-straight coastlines. A positive gradient in longshore transport between two cross-shore transects implies a reduction of the total amount of sand and therefore erosion between the two boundaries. A negative gradient the opposite: sedimentation (Steetzel, 1993). These processes are schematically illustrated in Figure 2.2. Coastal expansion is however generally not considered a problem, unlike coastal retreat.

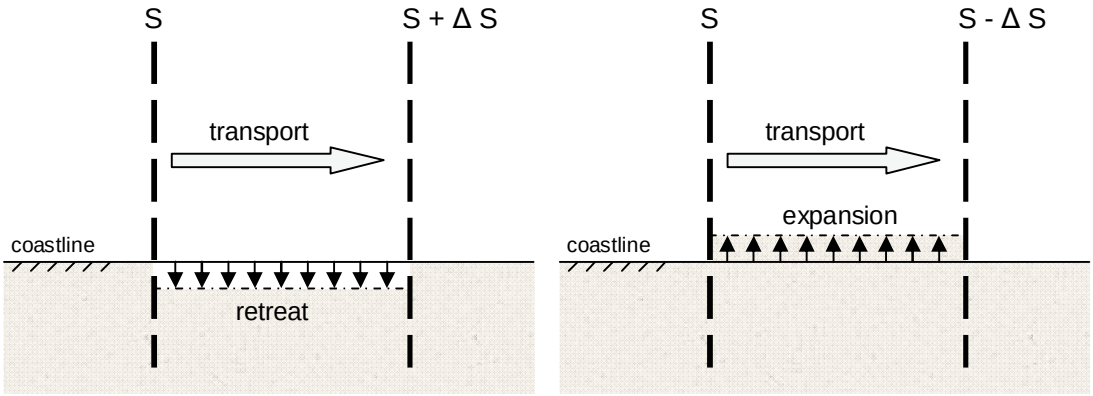

Figure 2.2 Schematic representation of shoreline retreat as a result of a positive longshore transport gradient (left) and of shoreline expansion as a result of a negative longshore transport gradient (right).

Long-term coastal erosion can also be accounted for by a net cross-shore transport, for example by sea-level rise. The cross-shore profile is then gradually reshaped and the dune face slowly shifts in landward direction, but no net sediment exchange takes place with adjacent areas.

2.1.2 Short-term erosion processes

On the short term, erosion of dune-fringed sandy shores takes place occasionally during less frequent events, when water level and waves are higher. Significant profile changes are in that case restricted to the upper part of the coastal profile (beach and dune) and take place in a matter of hours. The new profile will approach, as much as possible in the duration of the storm, the equilibrium profile corresponding with the storm water level and wave conditions, see Figure 2.3. During this reshaping process in a storm, the foreshore develops and waves will break further offshore. There is a decline in energy reaching the dunes and the erosion rate decreases with duration of the extreme conditions. Therefore most erosion takes place during the first period of a storm.

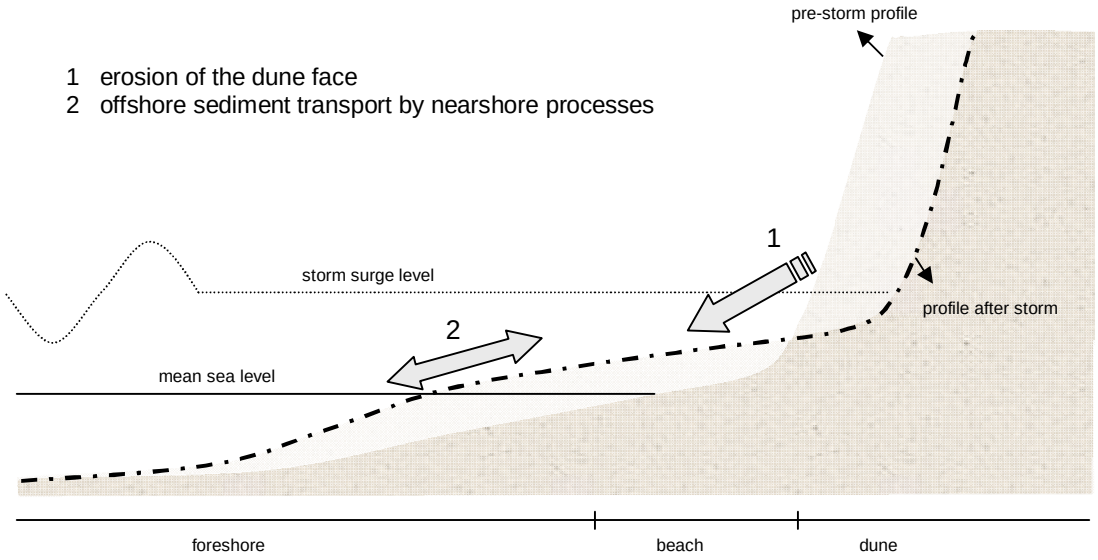

Figure 2.3 Schematic representation of the transformation of a dune during storm surge. The pre-storm profile is gradually reshaped, approaching the equilibrium profile corresponding with the water level and wave conditions during the storm.

In absence of a longshore transport gradient, the total amount of sand between two cross-shore arrays is not affected. Only reshaping of the profile takes place. The new profile is in this case only temporary, as under the following normal conditions the pre-storm profile is gradually recovered. When there is a positive transport gradient present, the sediment that is deposited on the beach will be transported in longshore direction. The dune profile is then never recovered, implying a shoreline retreat.

2.2 Dune face erosion mechanisms under storm conditions

According to Nishi and Kraus (1996), there are three types of erosion mechanisms of sand dunes by wave impacts during storms or strong wave action. These cross-shore dune erosion mechanisms, schematised in Figure 2.4, are classified as (a) layer separation, including layer separation and overturning, (b) notching and slumping, and (c) sliding and flowing.

Layer separation (a) typically occurs if a near-vertical dune face is subjected to wave impact. Over the duration of a certain number of wave impacts, a vertical crack develops, and the outer layer gradually separates from the dune. As it separates, it either becomes unstable and collapses suddenly (a1), or tilts forward and overturns (a2). Severe notching (b) tends to occur when a dune face is nearly vertical, permeated by roots, highly compacted or composed by rock. Notching is limited to the elevation of the wave attack and, after the notch is cut deep enough into the base of the dune, the overlying sand column collapses. Sliding and flowing (c) occurs on uncompacted gently sloping dunes that have a face slope close to the angle of repose of the sediments forming them. In this situation, modest wave impact at the base of the dune or even exposure to rain and wind can cause a thin layer of sand to run down the slope. It is expected that this mode of erosion does not cause severe dune recession in a short period of time, however this mechanism tends to steepen the dune

face and a resultant steeper dune slope will probably trigger layer separation or notching and slumping under storm conditions.

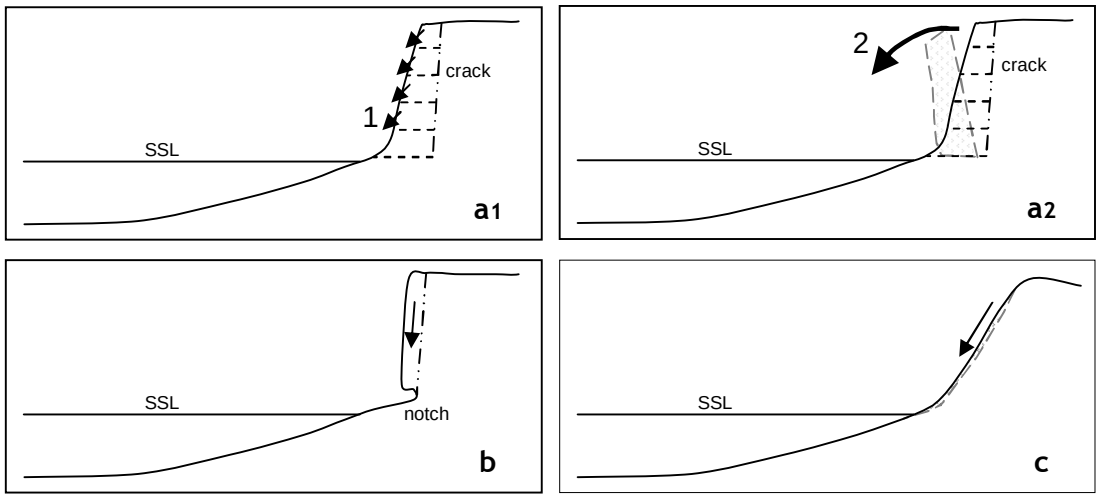

Figure 2.4 Dune erosion mechanisms during storm conditions, according to Nishi and Kraus (1996): (a1) layer separation, (a2) layer separation and overturning, (b) notching and slumping, (c) sliding and flowing

It is plausible that the occurring dune erosion mechanism is determinative for the relation between wave impact and sediment flux. It is thus important to identify the erosion mechanism for the situation studied and possible transitions between erosion mechanisms with progress of the storm or experiment.

3 Large-scale dune erosion experiments

Large-scale physical dune erosion tests were performed from November 2005 until February 2006 in the Delta flume, a research facility of WL | Delft Hydraulics. The general objective of the physical model tests was to quantify and gain insight in dune erosion and nearshore hydrodynamic processes of a coastal profile characteristic for the Dutch coast. The measurements obtained during these tests are used for this research.

3.1 Physical test setup

The scale at which the physical model was set up was aimed to be as close to prototype as possible to minimise scale effects. To translate the prototype situation to a model that fits in this flume, use was made of the scaling relations derived by Vellinga (1986). The scale relations were not used to translate model values back to prototype value. Consequently, all values presented in this report are model values.

3.1.1 Delta flume

The wave flume in which the large-scale physical model tests were carried out is the Delta flume of WL | Delft Hydraulics. The flume has an effective length, width and height of 225 m, 5 m and 7 m respectively. The wave generator is equipped with Active Reflection Compensation and 2nd order wave steering to take long waves and wave shape into account. Irregular waves with a wave height up to 1.9 m can be generated depending on the water depth and the wave period. The scale at which the tests could be performed were restricted by the dimensions of the wave flume and on the capacity of the wave generator in the flume given the coastal profile and the hydraulic conditions expected during an extreme storm event at the Dutch coast.

3.1.2 Coastal profile

The initial coastal profile which was used in all tests (see Figure 3.1) is based on a reference profile which is considered to be characteristic for the Dutch coast. This strongly schematised profile consists of one dune with its dune top located at NAP +15 m. The slope of the dune face is 1:3 and ends at NAP +3 m. From thereon the slope is 1:20 to a level of NAP. From NAP to NAP -3 m the slope is 1:70. From that point on seaward the slope is 1:180. No banks or channels are present in the foreshore. The initial profile derived from this reference profile and used in the tests is shown in Figure 3.1. It was constructed of sand with a diameter D_{50} = 200 μm and is for this research assumed to be homogeneous. All tests were carried out with a water depth of 4.5 m in the flume near the wave board.

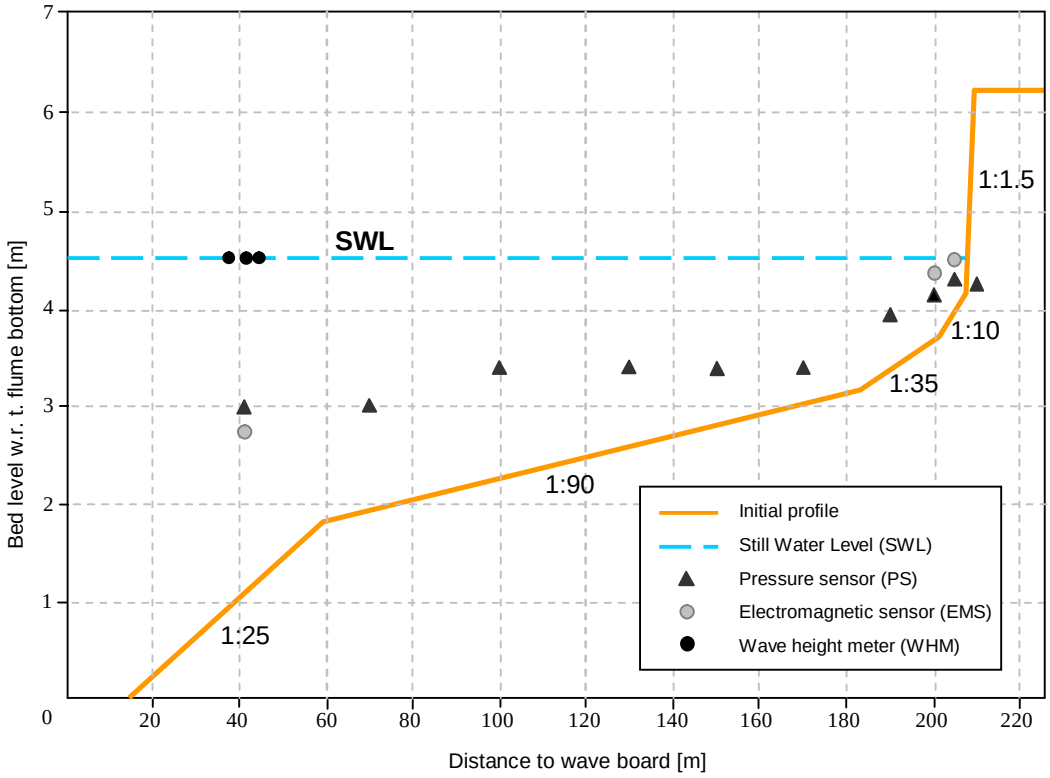

Figure 3.1 Desired initial profile and position of instruments fixed at the flume wall (WL | Delft Hydraulics, 2006)

3.2 Test program

Table B.1 shows the test programme with hydraulic conditions. The total duration of each test varied, but was at least 6 hours. In the first 6 hours the tests were temporarily interrupted to carry out bed profile measurements after the following fixed time intervals:

A. 0 until 0.1 hour
B. 0.1 until 0.3 hour
C. 0.3 until 1.0 hour
D. 1.0 until 2.04 hour
E. 2.04 until 6.0 hour

These will from now on be referred to as test parts. The duration of test parts increase as a test continues since erosion rates are highest at the start of the tests and decrease with the progress of a test due to the development of the foreshore, see Section 2.1. After 6.0 hours different hydraulic conditions were applied for varying durations, see also Table B.1. The test parts after 6.0 hours are indicated with characters in increasing alphabetical order. For test DP01 an additional test interruption occurred after 2.54 hours, due to sudden frost.

Tests DP02 and T08 will not be considered in this research. During DP02 no in-situ profile measurements were made during the first hour and no video measurements during the entire test, and the dune profile of T08 deviated from the other tests by an extra dune in front of the prototype dune. These two tests are therefore not mentioned any further.

3.3 Instrumentation and measurements

The devices that were used for the measurements required in this research are described in this section. These measurements are profile measurements done with both an in-situ profile follower and collected video images, and in-situ pressure and velocity measurements done with respectively pressure sensors (PS) and electromagnetic flow velocity sensors (EMS). The results of the measurements are also represented in this section.

3.3.1 In-situ profile measurements

To measure the entire profile from wave board to dune top between test intervals, both a mechanical amphibious profile follower, from hereon referred to as profiler (see Photo A.1), and an echo sounder are installed on a measurement carriage. The profile measurements are carried out before and after each test and after each test part in three cross-shore transects, always with water in the flume. One measurement is carried out along the longitudinal flume axis and the other two at 1.25 m on both sides of the flume axis. The profile measurement with the echo sounder is carried out only in the middle transect. The driving direction of the carriage is from the dune top to the wave board.

The measurement carriage drives over the rails on top of the walls of the flume with a maximum velocity of 0.15 m/s while the profiler is moving over the bed. A sample frequency of 30 Hz is applied and the samples are horizontally interpolated to steps with a length of 0.01 m. The profiler has a wheel with a diameter of 0.1 m and a width of 0.05 m.

The three parallel profiles measured by the amphibious profiler are averaged to one representative profile. In the averaging procedure each of the three measurements has the same weight. It should however be kept in mind that the average profile measurement does not give reliable information on profile features that vary strongly in cross-flume direction.

3.3.2 Video measurements

In addition to the in-situ profile measurements, near-shore bathymetry can also be measured using Argus cameras (Holland *et al.*, 1997) in combination with stereo video technique. This technique introduces the possibility to reconstruct the beach and dune face at any moment during the tests, as explained further in this section.

Video data were obtained with four cameras in Tests T05, T06 and DP01. During tests T05 and T06, all cameras operated with a sample frequency of 2 Hz, while in DP01 only two cameras recorded video data with a sample frequency of 4 Hz. Running cameras were synchronised by coax cables using an 11 volt trigger signal. Synchronisation with in-situ measurements was realised within video sample frequency using a small led light visible in one of the cameras that illuminates as the in-situ measurements were started.

The cameras were connected with a data computer by fire-wire cables intersected by hubs. The images were first stored on a data computer and then compressed to a jpeg-format and copied to a stand-alone hard disk. The jpeg-files are stored under a name containing a time indication in epoch-time, which is the exact time of storage in seconds since January 1, 1970, 00:00:00h.

Two cameras (referred to as cameras C1 and C2) were fixed to the roof of the flume shed at approximately the centre line of the flume (see Photo A.3, Photo A.4). Both cameras were pointed in the direction of wave propagation and resolve bathymetries for an area covering about twelve meters in along flume direction and six meters in cross flume direction. The other cameras (referred to as cameras C3 and C4) were fixed on a crane at the end of the flume and are respectively 6.7 and 5.2 meters off the longitudinal flume axis. Both cameras look against the direction of wave propagation and were deployed to measure wave transformation through the inner surf and swash zone. The exact positions of the four cameras are listed in. The used coordinate system has its origin at the wave board (x = 0), the flume centre line (y = 0) and the top of the flume wall (z = 0), see Figure 3.2.

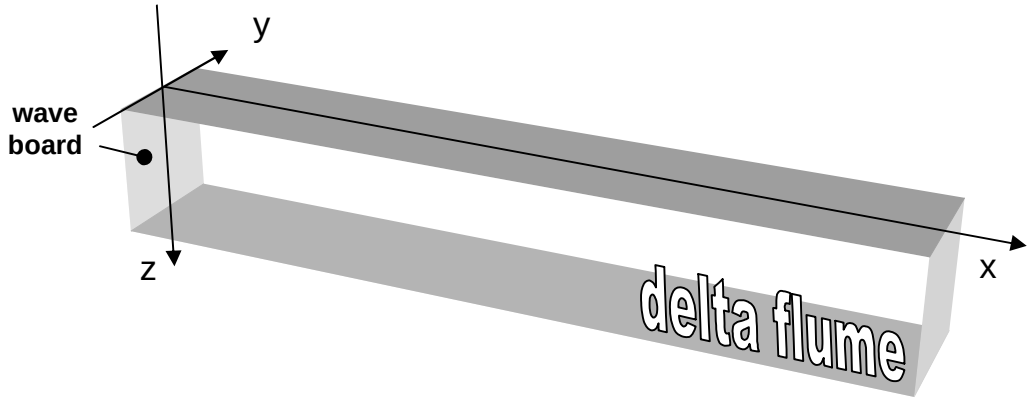

Figure 3.2 General conventions for a video coordinate system in the Delta flume

In order to compute camera geometries, defined as internal and external camera properties, use is made of so-called ground control points (GCP's). GCP and camera coordinates are input to a software program called *geomtool* (Holland et al., 1997) that generates the camera properties listed in Table 3.1. In total 17 GCP's are available, mostly being bolts on the flume rail.

Table 3.1 Camera locations and properties

Camera	*x* [m]	*y* [m]	*z'* [m]	Tilt [°]	Roll [°]	Azimuth [°]
C1	190.474	0.032	8.331	55.06	-87.62	89.49
C2	196.811	0.022	8.312	45.98	-90.58	91.40
C3	228.225	6.690	6.500	--	--	--
C4	228.198	-5.151	6.459	--	--	--

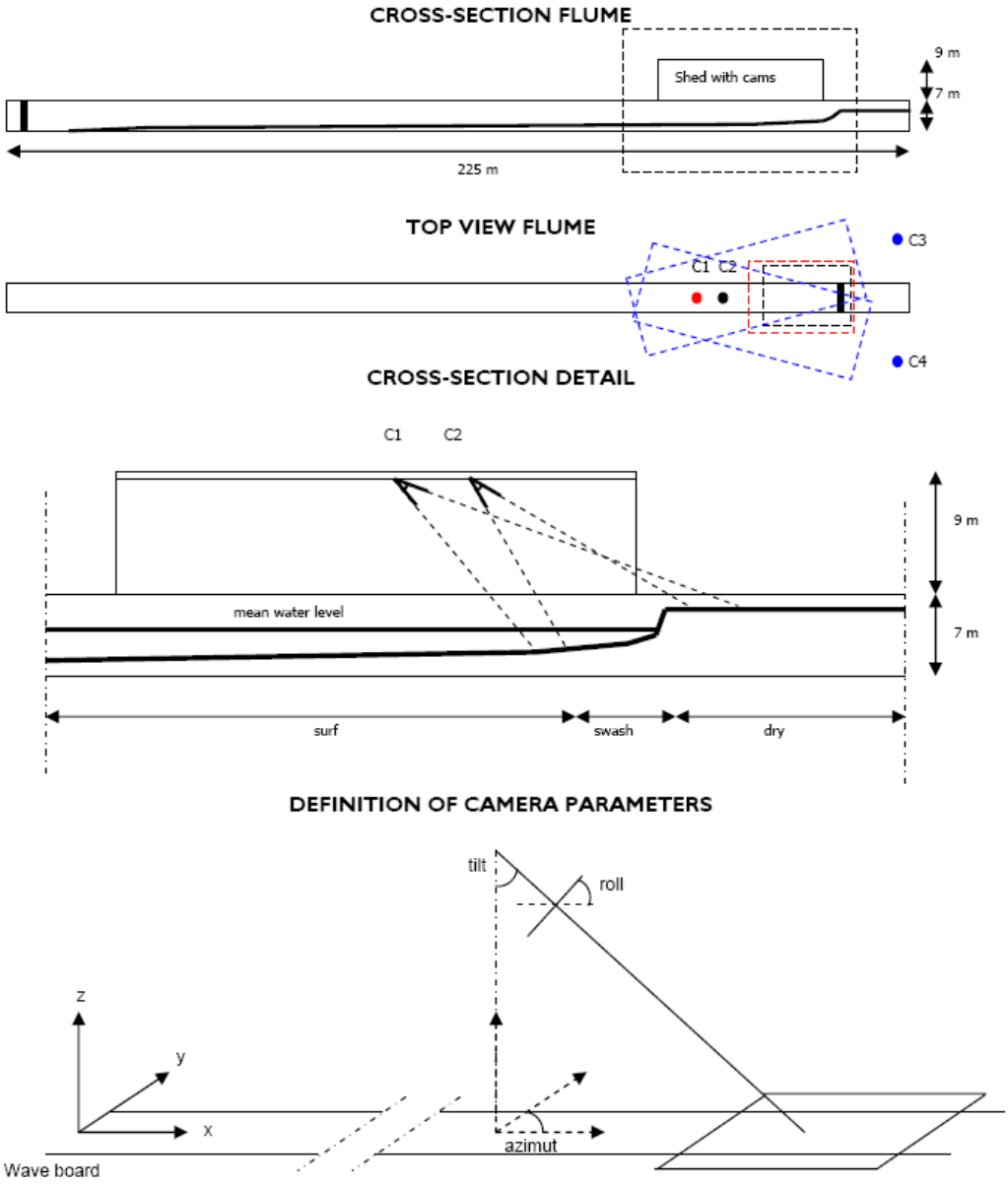

Figure 3.3 Camera configuration and definition of camera parameters for the video measurements in the large-scale Delta flume experiments

Stereo video technique introduces the possibility to reconstruct the beach and dune profile at any moment during the tests. To that end, images from cameras C1 and C2 taken on exactly the same moment are linked. The images are processed such that each pixel of one image is matched with a pixel in the second image that is in reality the same point in space. A predefined number of GCP's are also detected in the images. Using information on position and properties of the cameras (see Figure 3.3) and position of the GCP's, (*x*,*y*,*z*)-coordinates are calculated for the point considered. This is done for all pixels in the image. The 3D-profile is then obtained by interpolation of the *z*-values on a regular grid with a spatial resolution of 0.01 m in both *x*- and *y*-direction. Finally, the interpolated profile is combined with colour information from original images, resulting in images as in Figure 3.5 (Van Thiel de Vries *et al.*, 2006). For more detailed information on the stereo video technique is referred to Clarke *et al.*, 2007 (in preparation).

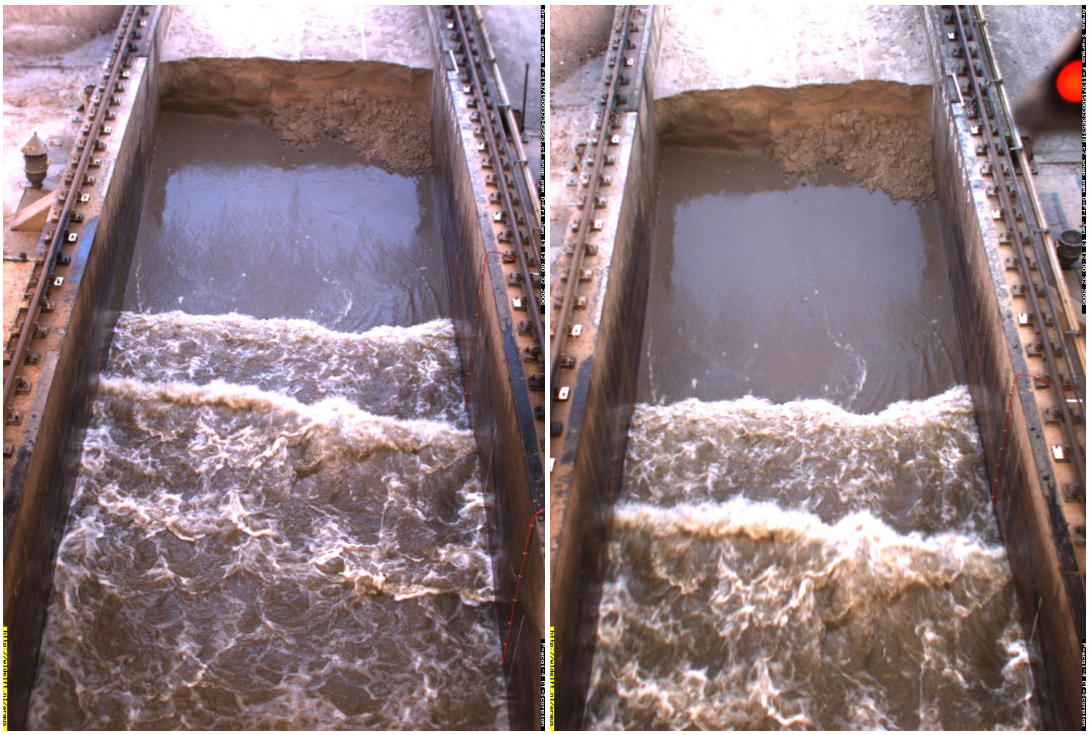

Figure 3.4 Snapshots of the same moment in test T06E by camera C1 (left) and camera C2 (right). In the upper part of the images the dune face is visible. The led light captured in the image of camera C2 is used to synchronise video images with in-situ pressure and velocity measurements.

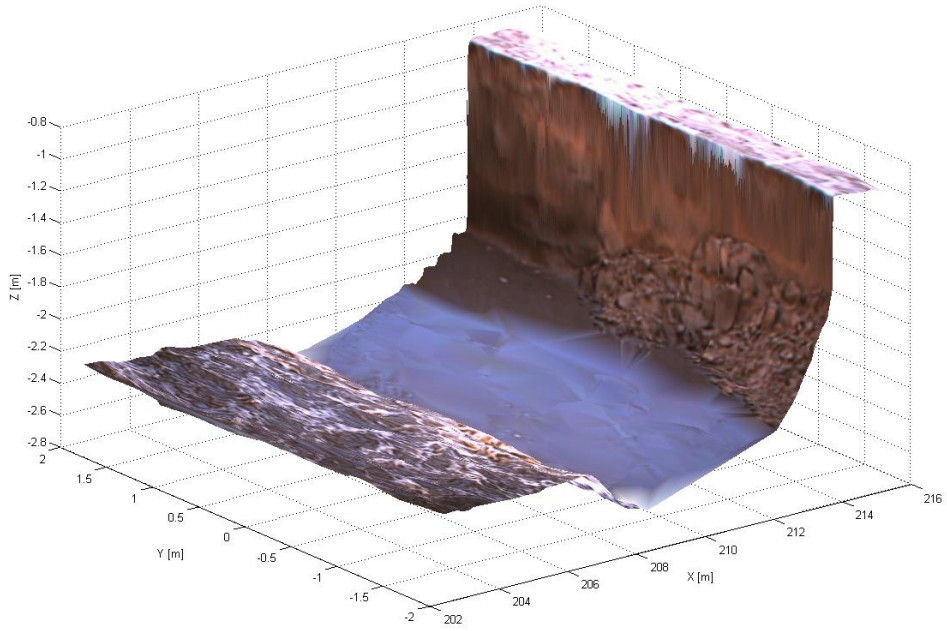

Figure 3.5 3D-plot of the dune and beach profile derived from the images in Figure 3.4 using stereo video calculations. The value of *z* on the vertical axis is with respect to the top of the flume wall.

It appears that the quality of a significant share of the video images was insufficient to properly reconstruct dune and beach profiles. The light intensity of the beach and dune face seems to be too low, resulting in low contrast and few distinct features on the dune face. As a result, too few pixels could be stereo matched between corresponding images. Due to this problem the profiles corresponding with only nineteen of the forty-three slump moments could be reconstructed. The dune top, including the dune crest, was however well reproducible for most images. This allows for an alternative method to calculate representative erosion volumes, as will be explained in Section 4.3.1.

3.3.3 In-situ pressure and velocity measurements

To obtain data on hydraulic conditions over the entire profile, a cluster of instruments was deployed on the flume wall. Wave conditions were measured with three resistance-type wave height meters, ten pressure sensors and three electromagnetic flow velocity sensors, see Figure 3.1. The position of the sensors can be found in Table 3.1 and Table 3.2. All pressure sensors and electromagnetic current velocity meters had a sample frequency of 25 Hz during tests T01 to T03. In tests T05, T06 and DP01 a sample frequency of 20 Hz was applied.

Table 3.2 Positions of pressure sensors fixed to the flume wall (WL | Delft Hydraulics, 2006)

Pressure sensor	Distance from wave board [m]	Distance from flume bottom [m]
PS01	41	3.00
PS02	70	3.00
PS03	100	3.40
PS04	130	3.40
PS05	150	3.40
PS06	170	3.40
PS07	190	3.95
PS08	200	4.15
PS09	205	4.30
PS10	209	4.25

Table A.1 Position of current velocity sensors fixed to the flume wall (WL | Delft Hydraulics, 2006)

Flow velocity sensor	Distance from wave board [m]	Distance from flume bottom [m]
EMS01	41	2.90
EMS02	200	4.35
EMS03	205	4.50

For this research, it is recommended to use the closest collocated pressure and velocity sensors with respect to the dune toe, as it is desirable to calculate wave impact at the location of the dune face. Wave impact per time step is derived from pressure and velocity (see Section 4.3.2). This implies the use of pressure sensor PS09 and velocity sensor EMS03

at 205 m from the wave board. However, these sensors are frequently above the water level during the tests. Pressure sensor PS08 and EMS02, both located at 200 m from the wave board (see Table 3.1 and Table 3.2), give better results and will be used for this research. It should however be kept in mind that these measurements deviate from the actual values of pressure and velocity at the dune face. Velocity sensor EMS02 is also sometimes above the water level, resulting in sharp spikes in the horizontal flow velocity. The datasets of EMS02 are therefore post-processed to despike the results.

3.4 Test results

The dune profile changes during the tests from the initial profile into a profile resembling an equilibrium profile corresponding to the storm surge level (see also Figure 2.3). This profile change takes place very fast at the start of the test, and gradually slows down. The toe of the dune face is initially below SWL. Erosion starts at the toe of the dune face where the slope becomes steeper until it is nearly vertical. The dune toe moves upward and is above SWL after 0.1 hour. The dune face then gradually moves in landward direction. The height of the dune face decreases with continuation of the experiment, as the dune toe moves upward while the top of the dune remains on a constant level. These observations are confirmed by the figures in Appendix C, showing the development in time of the average of the measured cross-shore profiles in all tests. One example is given in Figure 3.6. The eroded sediment is deposited in the area in front of the dune. The profile only showed a considerable development in a relatively small part of the entire profile in the flume between about 170 m and 215 m from the wave board. The rest of the profile did not significantly change during the tests.

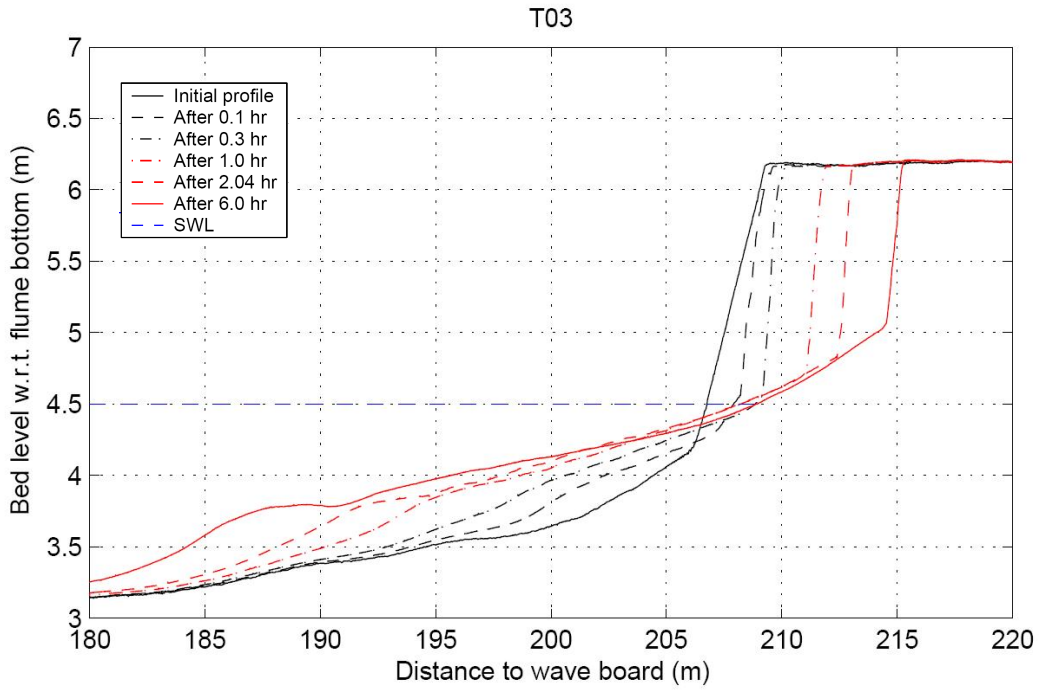

Figure 3.6 Development of average cross-shore profile for test T03, derived from the three in-situ measured profiles after each test part.

The dune erodes episodically by lumps of sediment falling off or sliding down the dune face. Under wave attack the dune face is continuously steepened (sliding and flowing) until the dune face is nearly vertical or even overhanging (notching) and a lump slides down the dune face (slumping). It can be concluded that a combination of the second (b) and third (c) erosion mechanism occurs during the tests, see the theory by Nishi and Kraus (1996) on dune erosion mechanisms in Section 2.2. According to their theory, notching mainly occurs when a dune face is nearly vertical, permeated by roots, highly compacted or composed by rock. Apart from the nearly vertical dune face, these conditions do not agree with the conditions of the dune in the Delta flume experiments. Still, it appears that the visually observed erosion mechanism of lumps sliding down the dune face corresponds with mechanism (b).

The moment that a lump of sediment falls down does not always coincide with the moment of a wave being in contact with the dune face. Often there is some time between the last wave contact and a slump event. The length of the lumps in cross-flume direction is always smaller than the entire width of the flume but mostly exceeds one third of the flume width. In the along-flume direction the length is about 0.1 to 0.3 m. Once these lumps fall apart on the beach the sediment is gradually transported away from the dune, steepening the dune face again, see Figure 3.7.

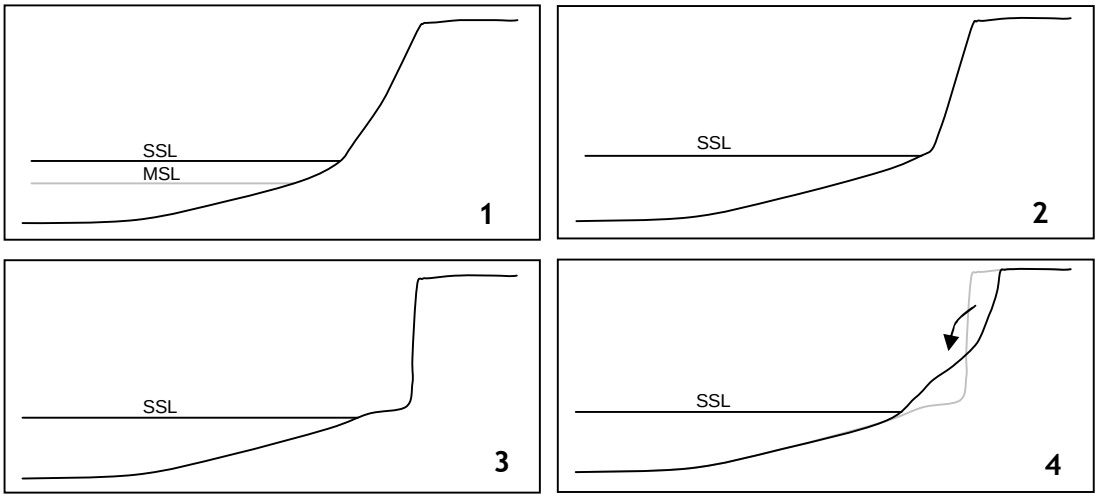

Figure 3.7 Schematic representation of the steepening and slumping process of the dune face under wave attack as observed during the dune erosion experiment in the Delta flume.

As a result of a slump event, lumps of sediment on the upper part of the beach temporarily block a part of the dune face, therewith protecting it from direct wave attack. The part of the dune face that is still entirely exposed to waves is at that moment more vulnerable for erosion than the obstructed part. This process seems to reduce the variations of the erosion profile in cross-flume direction, implying that time-averaged retreat area of the dune face is uniform over the width of the flume. The period of time needed to remove a sediment lump from the beach is shorter at the beginning of the tests than at the end of the tests. At the end of the tests, the waves do not reach the dune face anymore and the dune profile is nearly constant. The decline in wave impact in time is visible in Figure 3.8. How this wave impact is derived is explained in Section 4.3.2.

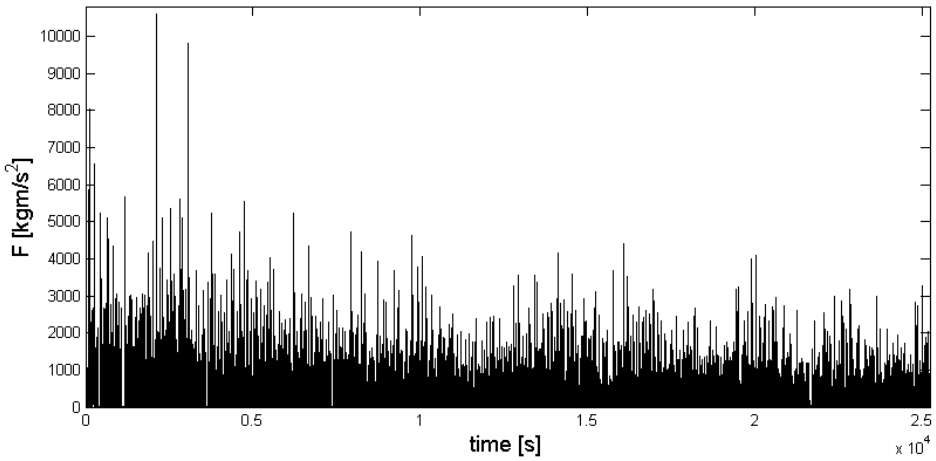

Figure 3.8 Wave impact in time for test DP01, derived from measurements at pressure sensor PS08 and flow velocity sensor EMS02.

The decrease of slump frequency in time can be recognised in the time stacks in Figure 3.9. In these time stacks, one predefined pixel array parallel to the v-axis of the images (perpendicular to the dune face) is taken from each image of one camera during an experiment. In such a pixel array, there is a distinct transition in light intensity between the dune top and the beach, clearly marking the crest of the dune. When the pixel arrays are stacked in time, an image is created which gives information on the location of the dune crest in time.

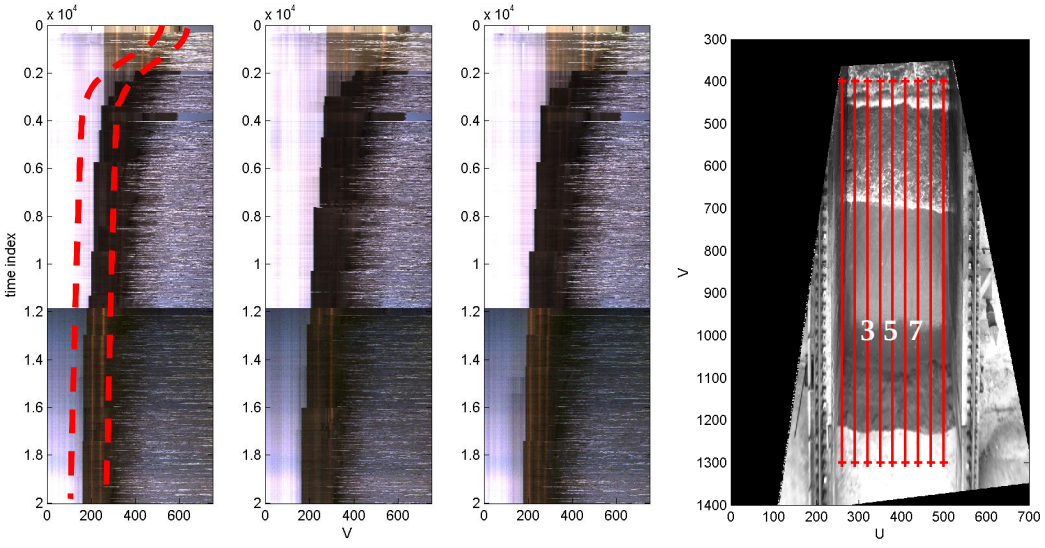

Figure 3.9 Left: time stacks for three transects in cross-shore direction comprising the first two hours of test DP01. The fast retreat of the dune face at the start of the test and the decrease in slump frequency with progress of the test are clearly visible. Right: rectified image with transects used to generate time stacks the three transects for which these time stacks are made (Van Thiel de Vries, 2006).

In visual observations the size of the sediment lumps did not seem to vary much in time: at the beginning of the tests (after 1.0 hour) the size was roughly the same as at the end of the tests (WL | Delft Hydraulics, 2006).

Cross-shore profiles can be plotted using the calculated (*x*,*y*,*z*)-coordinates from stereo video observations (Clarke *et al.*, 2007 (in preparation)). Plotting a cross-shore profile just before and just after a slump event (see Figure 3.10) reveals that slump events indeed take place as described in Figure 3.9. The upper part of the dune face slides down onto the beach just in front of the dune.

A series of cross-shore profiles can be plotted for the period between two slump events, see Figure 3.11. The profiles were plotted for one transect where two slump events took place relatively short after each other and for time intervals in the order of a minute. Steepening of the dune face as visually observed during the tests is also clearly visible in this plot. The steepening process mainly consists of relocation of sand deposited by the previous slump.

The main findings on the dune erosion processes during the experiments that can be drawn from these observations are:

- The cross-shore profile shape changes in time into a near-equilibrium profile corresponding with the present hydraulic conditions
- This profile change takes place very fast at the start of the test, and gradually slows down
- The toe of the dune face is partly located below SWL at the start of the tests but is elevated entirely above SWL in the first minutes of the tests
- The erosion mechanisms during the experiments are both (b) notching and slumping and (c) sliding and flowing (Nishi and Kraus, 1996, see Section 2.2)
- Slumps do not take place over the complete width of the flume
- The time-averaged dune crest retreat is uniform over the width of the flume
- The slumping frequency decreases in time
- The slump erosion volumes do not seem to decrease in time
- The number of waves reaching the dune face decreases with the development of the cross-shore profile

And from these findings another one can be drawn:

- The decrease in erosion rate, expressed in the gradually stabilising cross-shore profile shape, seems to be a result of the increasing time interval between slump events, not a result of a decrease in slump erosion volumes

This can however not be concluded from these observations as such.

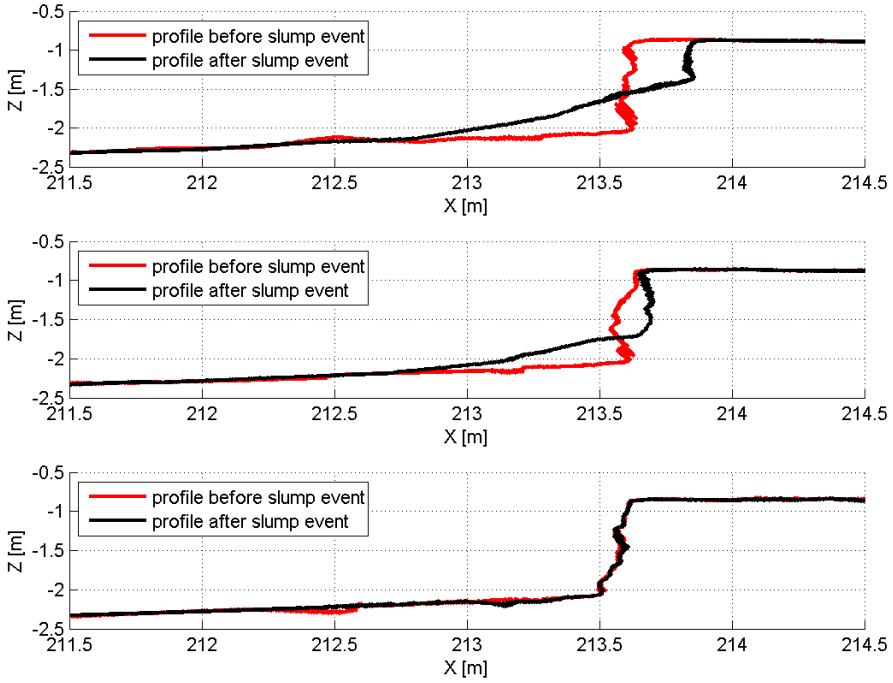

Figure 3.10 Profiles for three cross-shore transects derived from video images taken at the moments just before and just after the slump event in T06E as shown in Figure 3.5. The second graph shows profiles for the longitudinal flume axis, while the other are at 1.25 on both sides of this axis. The profiles in the top graph reveal that the slumping mechanism indeed takes place as described in Figure 3.9.

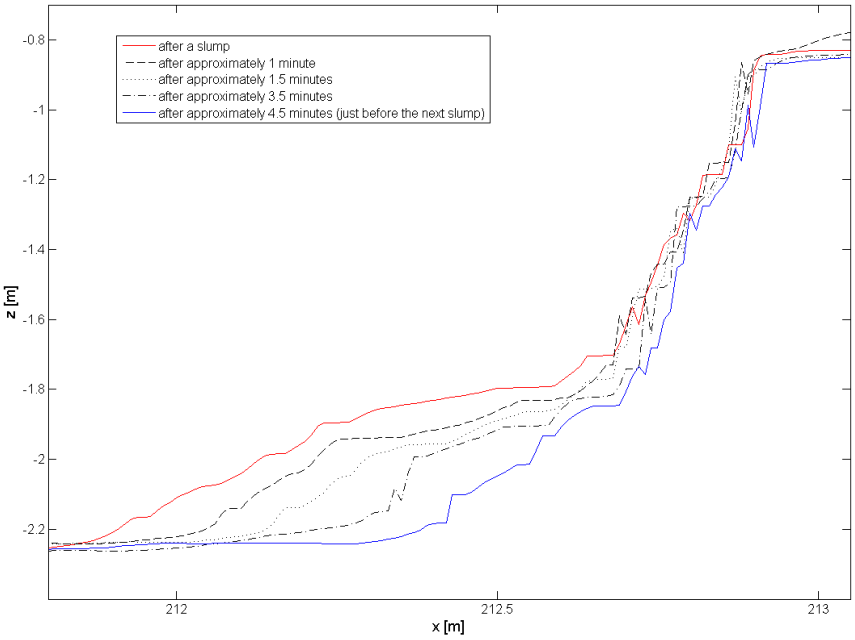

Figure 3.11 A series of cross-shore profiles between two slump events in test T05D with individual time intervals in the order of a minute, derived from stereo video data. The red line is the profile just after a slump event while the blue line is the profile just before the next. .

4 Wave-impact driven dune erosion model

4.1 Different approaches in dune erosion modelling

Several approaches exist to model dune erosion under given hydraulic conditions. These can generally be divided into equilibrium profile approaches and process-based approaches. The first assumes that the beach profile strives towards an equilibrium state defined by the wave and water level conditions, which geometrically determines the response of the dune (Vellinga, 1986, Kriebel and Dean, 1993). Process-based models describe sediment fluxes on the dune and in the swash zone in time such that the morphodynamic response of the dune and beach under given hydraulic conditions is predicted. One process-based approach relates dune face erosion and swash zone transports to the capacity of nearshore flows to transport sediment offshore (Steetzel, 1993). A second process-based approach is the wave impact approach which estimates the sediment transport from the dune as a result of the impact of the waves directly hitting it (Fisher *et al.*, 1986). This latter model decouples inner surf and swash zone sediment transports from dune face erosion, enabling a combination of the wave-impact driven model with a process-based morphodynamic model for the nearshore. Such a combined model allows for a physical feedback between nearshore hydrodynamics, dune face erosion and the evolution of the foreshore and nearshore from that erosion. It is therefore desirable to develop a wave-impact driven dune face erosion model similar to the one by Fisher *et al.* (1986), but taking into account the phenomenon of slump events.

The approach by Fisher *et al.* (1986) is further elaborated on in the next section. Section 4.3 presents an altered approach on wave-impact driven dune face erosion modelling. This approach describes sediment flux as a function of frequency and magnitude of slump events and wave impact as, among others, a function of the period the period during which waves attack the dune face.

4.2 Wave-impact driven dune face erosion model by Fisher *et al.* (1986)

In their study regarding a wave-impact driven dune erosion model, Fisher *et al.* (1986) examined the relation between incident wave force and dune face erosion volumes. They considered the total erosion of a dune during a storm as the summation of the individual erosion volumes resulting from the individual swash uprushes which impact the dune. The impact of an individual wave *SF* (specific force) was defined by the mean of the product of the leading edge velocity squared $u_{swi}^{\ 2}$ and the maximum bore height h_{swi} while it is in contact with the dune (Fisher *et al.*, 1986):

$$SF = \rho \overline{h_{swi} u_{swi}^2} \quad \left[N/m \right] \tag{4.1}$$

In flume experiments, one wave at a time was exerted on a scale model of a dune in a 12 m long wave flume. After each wave impact the eroded volume was geometrically determined. Leading edge velocity and bore height were measured with wave height and velocity meters. The results from flume experiments by Fisher *et al.* (1986) are presented in Figure 4.1.

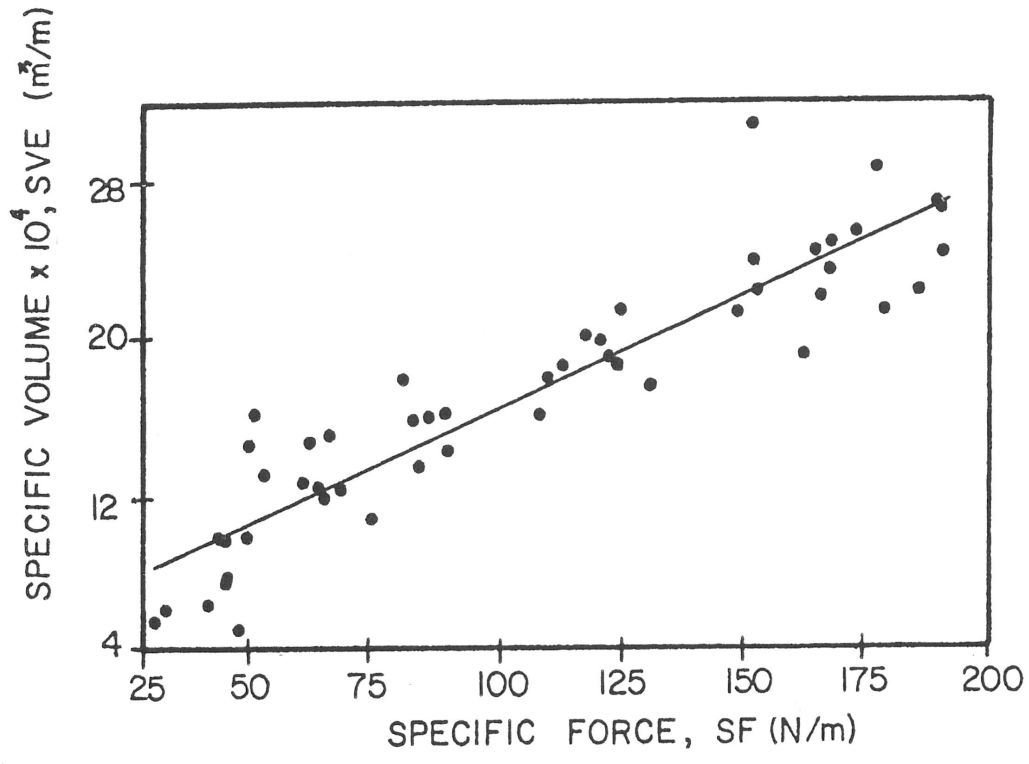

Figure 4.1 Linear correlation between specific force and corresponding specific volume eroded for laboratory dune erosion tests by Fisher *et al.* (1986).

The maximum force reached in the relatively small flume was rather small. Therefore also field experiments were done to determine whether a similar relationship could be found on a scale approaching prototype conditions. The field experiments consisted of a 1 m high constructed dune model between two vertical retaining walls on the beach, 1.3 m apart. The sand was compacted and saturated and the dune foot was positioned at mean tide level. During rising tide, velocity and bore height measurements were done in front of the dune, and individual erosion volumes as well as total erosion volumes were geometrically determined using a grid on the inside of the retaining walls and photographs taken at regular intervals during the tests. No attempt was done to do experiments during storm conditions. The relatively high water level and waves compared to the dimensions and level of the scale model on the beach were considered representative for storm conditions.

The results of the field experiment gave a considerable scatter and no significant relation between the force and the erosion, see Figure 4.2. According to Fisher *et al.* (1986), this was probably due to the noisiness of the field data and the difference in nature of the dune erosion: during the field experiments the shape orientation of the dune face continuously

changed in time with the rising tide level, while in the flume the face was nearly vertical throughout the experiments.

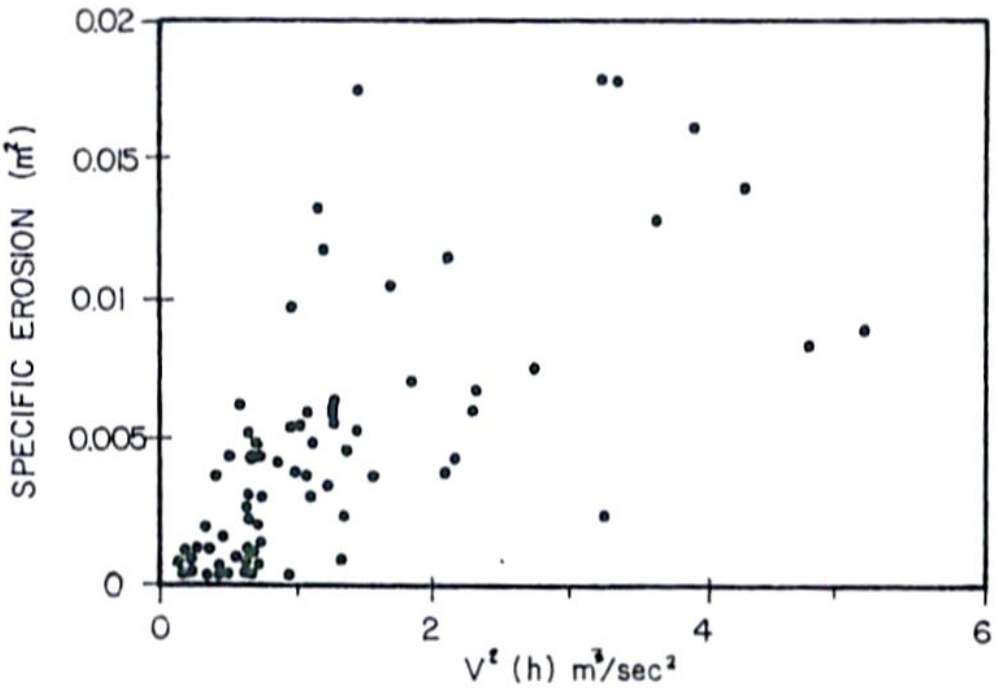

Figure 4.2 Results for incoming swash force $\overline{h_{swi}u_{swi}^2}$ and corresponding specific volume eroded in field experiments by Fisher *et al.* (1986).

Grouping the data in intervals of specific force reduced the scatter shown in Figure 4.2. Figure 4.3 shows the correlation using combined data for three experiments. There is an improved correlation between the specific erosion and the specific force when these data are grouped by these intervals. According to Fisher *et al.* (1986) the intervals smooth out the scatter associated with the individual surges and the irregular dune face. When viewed this way, the field data agree with the laboratory data in that there is a linear relation between the erosion and the wave forcing on the dune (Fisher *et al*, 1986).

Using the data from four reliable experiments, Fisher *et al.* (1986) also evaluated the cumulative effects of the swash by plotting the total specific erosion during an entire experiment against the summation of the individual specific force values, see Figure 4.4. As in Figure 4.3, these data also appear to be well correlated.

As can be seen in these figures, a linear relation was found from these flume experiments, for both the time scale of individual waves and of entire experiments. A linear relation is plausible as waves with high impact have, according to the given definition, either a high maximum bore height or a large leading edge velocity or both. Either way, these waves have a higher uprush and are therefore able to reach a larger area of the dune face and transport more sediment down the dune face.

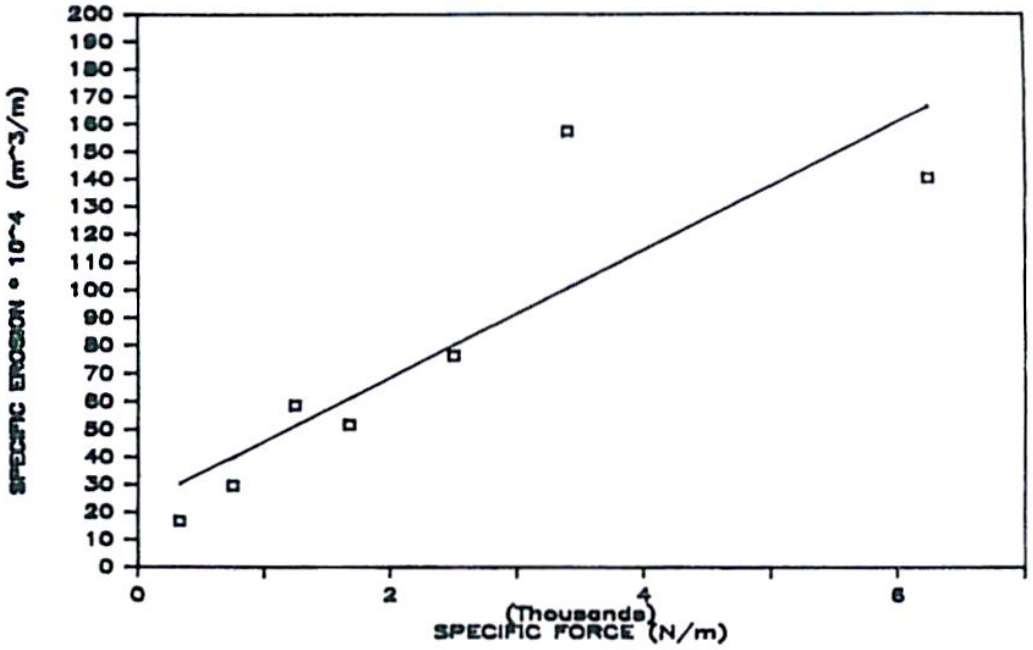

Figure 4.3 Results for specific force *SF* and specific volume *SVE* eroded in field experiments, grouped by intervals of wave impact.

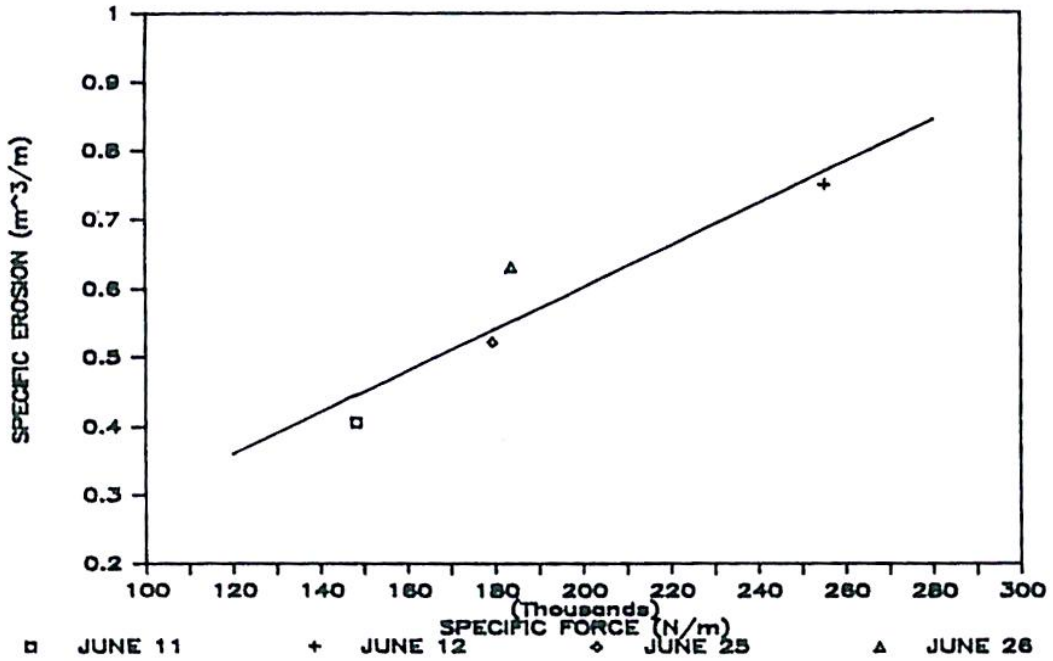

Figure 4.4 Total specific erosion vs. summation of specific force *SF* for four experiments in field experiments.

4.3 Dune erosion modelling

The approach by Fisher *et al.* (1986) considers the total dune erosion during a storm as the summation of the individual erosion volumes resulting from the individual swash uprushes which impact the dune. On the time scale of single waves as well as on the time scale of an entire storm Fisher *et al.* (1986) found a linear relation between wave impact and dune erosion volumes. Their approach however does not take the occurrence of slump events into account, while according to the test results (see Section 3.4) the sediment flux from the dune face appears not to be constant in time but highly correlated with the periodically occurring slump events. The fact that the correlation found by Fisher *et al.* (1986) was improved when grouping data in intervals of wave impact (see Figure 4.3) suggests that a time scale should be taken into account. It therefore seems logical to include the time scale of slump events in a wave-impact driven dune erosion model.

In this research, the relation between wave impact and sediment flux is studied taking into account the period ΔT of wave attack between slump events. Sediment flux is defined as dune erosion volume per unit of time $\Delta V/\Delta T$. Period ΔT by definition determines the frequency of slump events, as frequency f_s is the inverse of the period ΔT between the slump events.

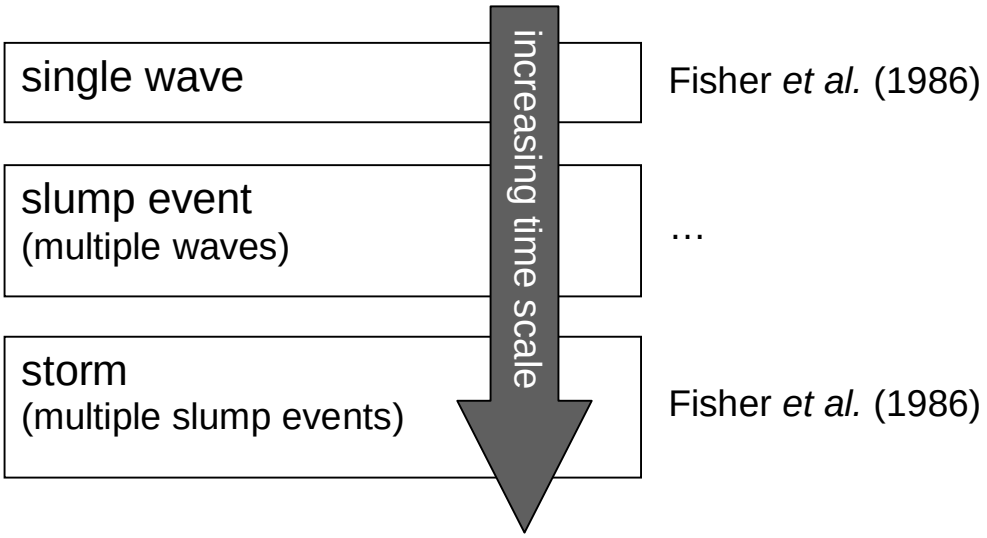

Figure 4.5 Representation of the time scales on which Fisher *et al.* (1986) studied the relation between specific wave impact and corresponding specific dune erosion volume. The time scale of single slump events is not considered in their approach.

Similar to the research of Fisher *et al.* (1986), it is interesting to study wave-impact driven dune erosion two time scales. Besides the time scale of slump events also the time scale of entire test parts is therefore studied. To be able to examine the relation between wave impact and sediment flux, dune erosion volumes and corresponding wave impact are first defined. This is done separately for the case of individual slump events and for entire test parts. Additionally, corresponding periods ΔT are defined. Values for erosion volumes, wave impact and periods and are subsequently derived from the datasets of the Delta flume experiments. This is described in the following paragraphs. Chapter 5 elaborates on the relations found with the results.

4.3.1 Definition of erosion volumes

To be able to couple a wave-impact driven dune erosion model with a swash zone sediment transport model, it is desirable to be able to express sediment flux and therefore erosion volume in terms of mass. Erosion volume should be defined such that the volume consists of sand with a porosity that can be considered homogeneous. This will allow for the conversion of volume into mass:

$$\Delta W = \Delta V \rho_s \left(1 - n_p\right) \quad \left[\frac{kg}{m} = \frac{m^3}{m^1}\frac{kg}{m^3}\right] \tag{4.2}$$

in which ρ_s is mass density of sand and n_p the porosity of the sand in the dune. In this research, only ΔV is considered. Parameters ρ_s and n_p are constants and the relation between sediment flux and wave impact based on volumes is proportional to the relation based on mass.

Two methods can be applied to define the erosion volume considering an individual slump event. Both methods are based on profiles at different stages of the slumping process, derived from stereo video observations. In the figures, profiles are numbered according to the following definitions:

1) Profile just before the slump considered
2) Profile just after the slump considered
3) Profile just before the next slump event

Method 1: Volume lost from the dune face during a slump

During a slump a certain volume of sand drops onto the beach. The sand mass lost from the dune face equals the mass added to the beach. This approach to erosion volume definition is desirable when the instantaneous volume of sand lost from the dune face as a result of a slump is of interest. The difference between post- and pre-slumping 3D-profiles then determines the erosion volume.

Method 2: Volume released into the active zone as a result of a slump

A second method to define erosion volumes is to consider the volume of sand released into the active swash zone as a result of a slump event. This method is based on the fact that the next slump occurs at the stage when a critical steepness of the dune face is reached again. The volume released into the active swash system is then determined by the difference between the profile just after a slump event and the profile just before the next, see Figure 4.7.

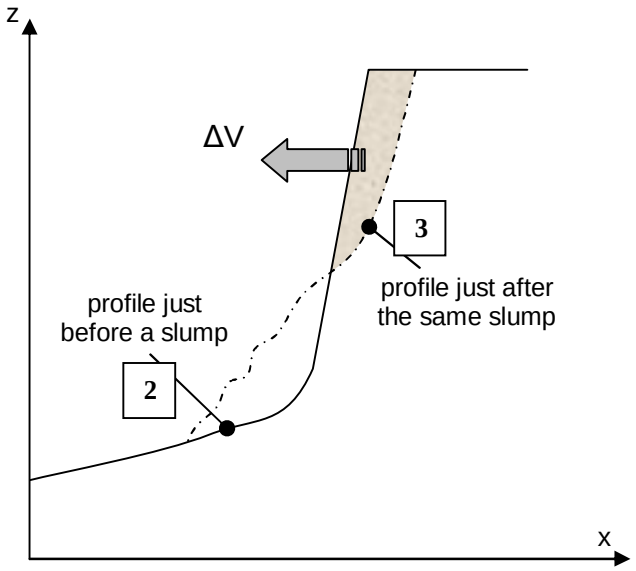

Figure 4.6 Definition of dune erosion volume when method 1, the sand volume lost from the dune face during a slump event, is considered.

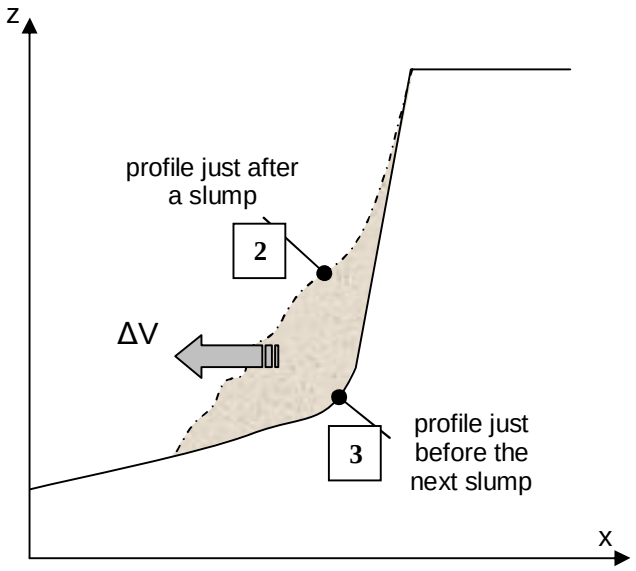

Figure 4.7 Definition of dune erosion volume when method 2, the sand volume released into the active system as a result of a slump, is considered.

Volumes of sand that fall apart on the beach have unknown variable porosities. Subtracting a profile just before a slump from the profile just after the previous slump results in a volume consisting of two parts with different porosities: the roughly known porosity of the sand in the dune and the unknown porosity of the sand volume deposited on the beach. The actual sand mass added to the active beach can thus not be derived using this method.

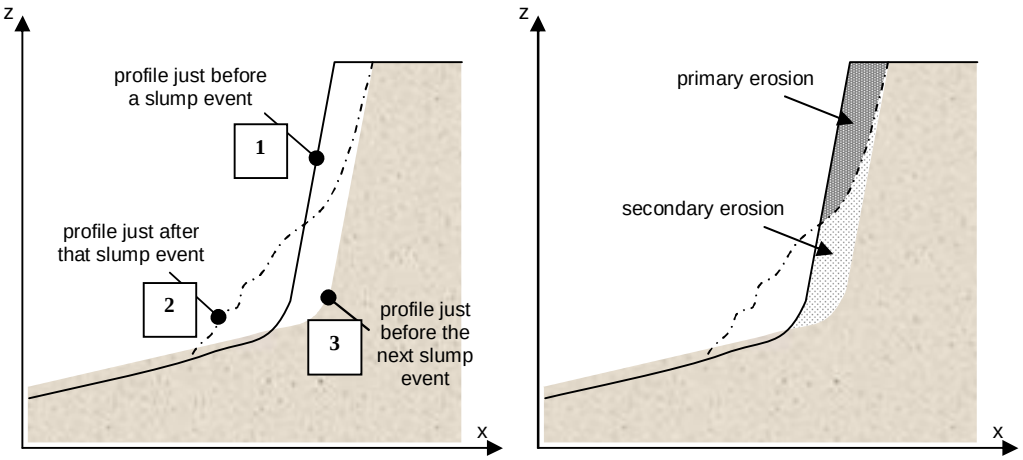

Figure 4.8 Left: definition sketch of the different stages in the erosion process when assuming the slumping mechanism. Right: definition sketch of primary and secondary erosion volumes.

An alternative approach is found to determine the volume added to the active swash zone as a result of a slump event. In this approach the profile just before the next slump event is subtracted from the profile just before the one considered (see Figure 4.9). In this manner, the volume has a homogeneous porosity and the mass of sand can be calculated when the porosity of sand in the dune is known. This method therefore seems to be appropriate for this research.

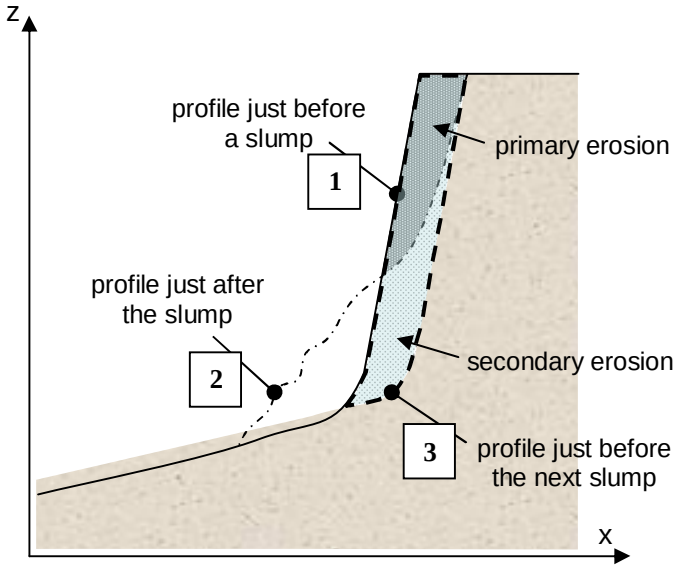

Figure 4.9 Definition of dune erosion volume when method 2, the sand volume released into the active system as a result of a slump, is considered. In this manner, the entire volume consists of equal porosity, allowing for conversion into sand mass.

For this research, total erosion volumes are calculated according to Figure 4.9 in method 2. When these volumes are derived from video data and cumulated for all slumps in a test part, the total eroded volume approaches the erosion volume for the entire test calculated with in-situ measured profiles, see Figure 4.10.

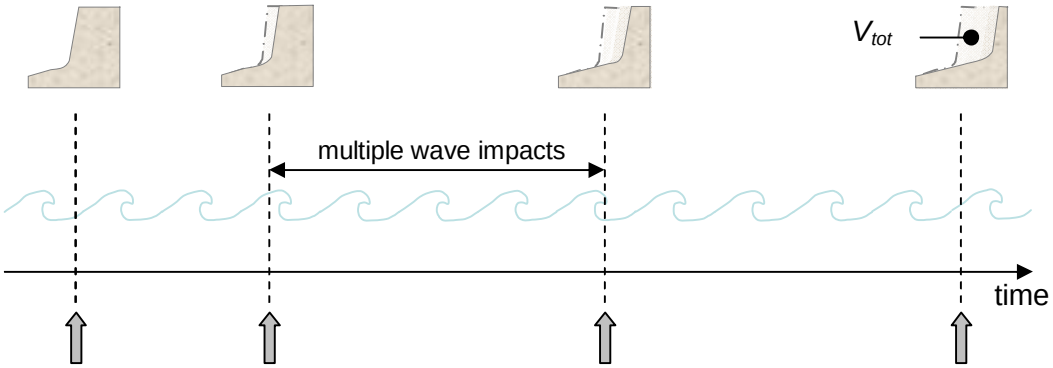

Figure 4.10 Schematic representation of consecutive slump events and the corresponding development of the dune profile. The dune profiles in the top of the figure represent the dune face profile just before the slump takes place.

The total dune erosion volume for an entire test part is defined as the width of the flume times the difference between the average profile at the start of the test part and the average profile after the test part. Only the landward side of the point where these profiles cross is taken into account, see Figure 4.11. Table E.1 shows the calculated dune erosion volumes V_{tot} using this definition and the average of the in-situ measured profiles between test parts.

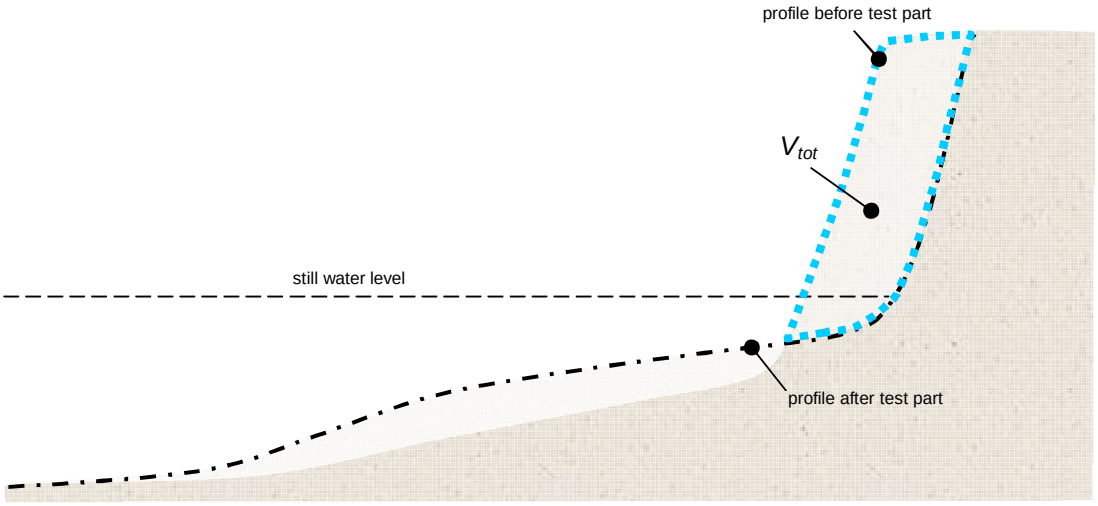

Figure 4.11 Schematic representation of the erosion volume V_{tot} per meter width during an entire test part.

Total erosion volumes for individual slump events are derived from video measurements. However, as not all video images allow for proper profile reconstruction (see Section 3.3), an alternative approach is necessary to calculate a representative erosion volume according to the definition above. As the dune top and crest profile could be reproduced for nearly all slump events, retreat area can be used to represent the eroded volume during a slump event.

The retreat area is defined by the area on top of the dune that is lost as a result of a single slump event. This is shown schematically in Figure 4.12. A linear relation was found between this retreat area and the corresponding total erosion volume. Using this relation the

retreat areas found were expressed in individual erosion volumes. The results for both total erosion volumes and retreat areas are gathered in Table F.1.

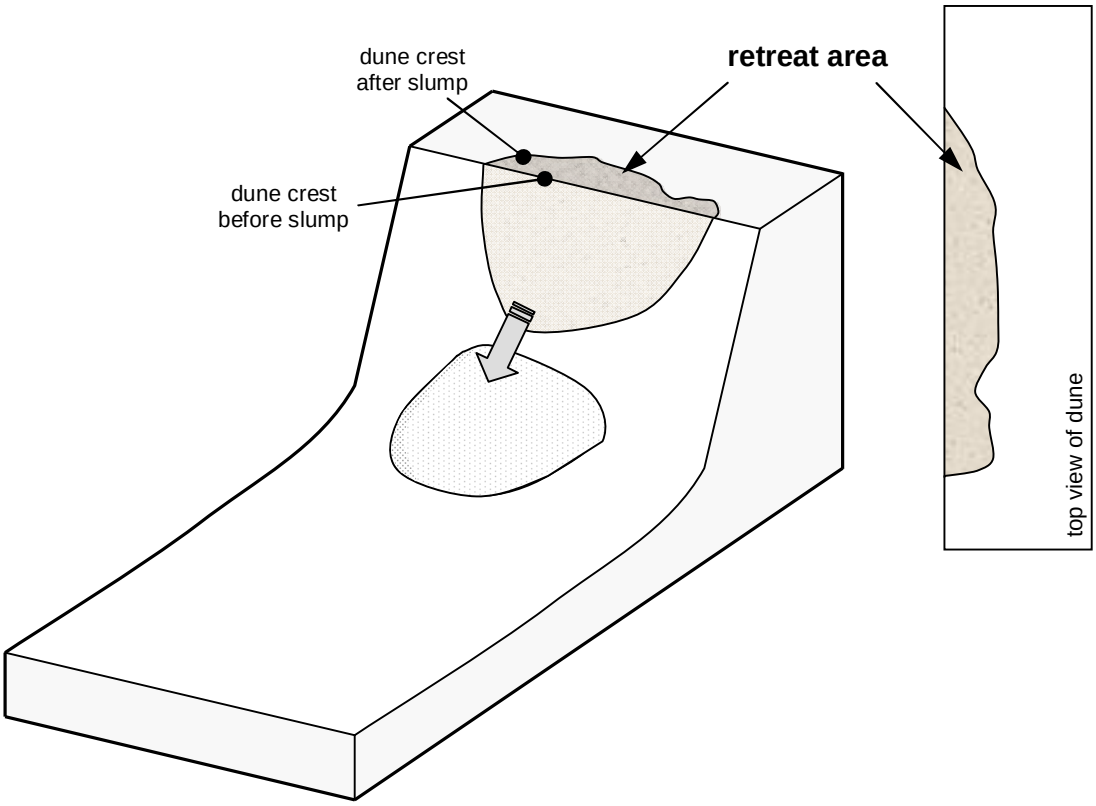

Figure 4.12 Definition sketch of the retreat area: the darker coloured area on top of the dune is the retreat area.

Primary and secondary erosion

According to the volume definition in method 2, a larger volume of sand is lost from the dune face as a result of one slump than the instantaneous volume displacement in the first method. This can be explained by introducing primary and secondary erosion.

After the sudden deformation of the dune face by the occurrence of a slump (primary erosion), the post-slumping profile will gradually transform again under the extreme wave conditions, until a second slump takes place, and so on. The post-slump dune face shape approaches the pre-slump shape again, while its location slightly shifts landward. To realise the transformation, a second volume of sand is displaced and redistributed over the beach, steepening the dune face again. This additional loss of sand is secondary erosion, see Figure 4.8.

Primary and secondary erosion are thus in fact different mechanisms occurring at the same time. Primary erosion is the slumping mechanism (b) as mentioned in Section 2.2 and takes place periodically. Secondary erosion is the sliding and flowing mechanism (c) and takes place continuously. The total erosion volume as in Figure 4.9, i.e. primary and secondary erosion together, does not distinguish between these two mechanisms. This should be kept in mind.

4.3.2 Definition of wave impact

Hydrodynamic processes and transformation of waves in the swash zone are very complex and for the most part yet unknown. There is no straightforward method to translate fundamental impact theory to waves colliding with a dune face. The approach used in this research is based on the one used by Fisher *et al.* (1986). They consider wave impact as the change in wave momentum during a certain contact period, where momentum is reduced to zero at the dune face. Fisher *et al.* (1986) defined the specific force of an incoming wave as change in momentum in terms of water level h_{swi} and leading edge velocity u_{swi} of the incoming bore:

$$SF = \rho \overline{h_{swi} u_{swi}^2} \tag{4.3}$$

The available datasets of the large-scale Delta flume experiments do not provide information on single waves. Wave impact is therefore primarily expressed as wave momentum change per time step, assuming that all wave momentum is reduced to zero at the dune face.

A broken wave travelling up the beach and impacting the dune face is schematised as a certain water column with water depth *h* derived from pressure measurements at PS08 and moving with a velocity equal to the flow velocity measured at sensor EMS02, see Figure 4.13.

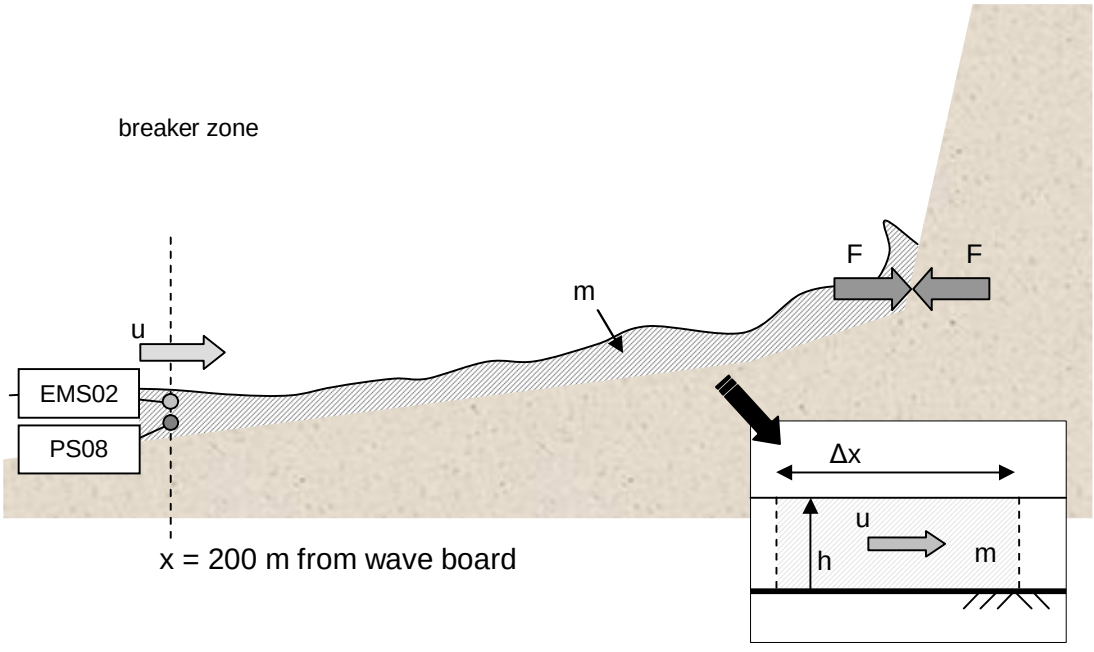

Figure 4.13 Schematic representation of the mass of a wave impacting the dune face. The mass of one wave is considered as the mass of a volume of water with constant height travelling over the beach with a constant speed *u* equal to flow velocity measured at the location of flow velocity sensor EMS02.

The wave impact or change in momentum Δp of travelling water mass per meter width of the flume during a sampling interval Δt is expressed in terms of flow velocity u, water depth h, water density ρ and period Δt.

$$F = \frac{\Delta p}{\Delta t} = \frac{\rho h u^2 \Delta t}{\Delta t} \tag{4.4}$$

where flow velocity u is measured at EMS02, and water level h is derived from pressure measurements at PS08. It is therewith assumed that the wave impact computed at PS08 and EMS02, approximately 10 m from the initial dune foot, is proportional to the wave impact actually hitting the dune for the complete duration of the tests.

This equation is only applicable in a strongly schematised situation. In fact, flow velocity u and water depth h are discrete datasets and variable in time. When measurements for flow velocity and pressure are done with sampling intervals Δt during a period ΔT, wave impact per meter width of the flume can be expressed in terms of water level h, flow velocity u and period ΔT with the following equation:

$$F = \frac{1}{\Delta T} \int_{t_1}^{t_1+\Delta T} \rho h(t) u(t)^2 \quad [N/m] \tag{4.5}$$

where $\Delta T = t_2 - t_1$ in which t_1 is the start of the period and t_2 the end. This definition resembles the one by Fisher *et al.* (1986) with an additional term to take into account the period during which waves exert the impact considered. Change in momentum for every time step is calculated, summed over all time steps in the wave period and divided by the period ΔT. This period can either be the time between two slump events or the duration of an entire test part.

As measurements for flow velocity and pressure are done with in-situ instruments in front of a dune, the effect of reflected waves is unquestionably present in the data. For calculation of the impact of a water mass travelling up the beach, only velocity and water level of incoming waves is required.

A method which has been used successfully in the field was presented by Guza et al. (1984). The method is based upon information from a co-located pressure sensor and a velocity sensor and uses shallow water theory to separate shoreward and seaward propagating long waves. Instantaneous surface elevation η w.r.t. SWL is derived from the in-situ measured pressure data and assumed to be a superposition of incoming (η_{in}) and outgoing (η_{out}) waves. The same is assumed for horizontal particle velocity u and discharge Q through a vertical plane perpendicular to the wave direction. Discharge per meter width of a flume can be defined as:

$$Q_{in} = c_g \eta_{in} \qquad \text{and} \qquad Q_{out} = \sqrt{g h_0}\, \eta_{out} \tag{4.6}$$

for respectively incoming and outgoing waves. c_g Represents the group celerity of the waves, h_0 is the still water depth and g the gravitational acceleration. With the assumptions above this results in a formulation for the incoming and outgoing surface elevation:

$$\eta_{in} = \frac{\sqrt{gh_0}\eta + Q_{in}}{c_g + \sqrt{gh_0}} \qquad \text{and} \qquad \eta_{in} = \frac{c_g\eta - Q_{out}}{c_g + \sqrt{gh_0}} \tag{4.7}$$

When assuming shallow water $c_g = c = \sqrt{gh_0}$ can be substituted in the equation. Using also relations $\eta = \eta_{in} + \eta_{out}$ and $u = u_{in} + u_{out}$, Equations (4.7) are reduced to:

$$\eta_{in} = \frac{\eta + u\sqrt{\frac{h_0}{g}}}{2} \qquad \text{and} \qquad \eta_{out} = \frac{\eta - u\sqrt{\frac{h_0}{g}}}{2} \tag{4.8}$$

and an expression is found for the incoming and outgoing flow velocity u_{in} and u_{out}:

$$u_{in} = \eta_{in}\sqrt{\frac{g}{h_0}} \qquad \text{and} \qquad u_{out} = \eta_{out}\sqrt{\frac{g}{h_0}} \tag{4.9}$$

As only incoming waves are considered in this research, u_{in} and η_{in} are used for the calculation of wave momentum. Taking into account only incoming wave signals according to Guza et al.(1984), the final expression for mean wave impact on the dune face becomes

$$F = \frac{1}{\Delta T}\int_{t_1}^{t_1+\Delta T} \rho h_{in}(t)\,u_{in}(t)^2 \quad [N/m] \tag{4.10}$$

4.3.3 Definition of period ΔT

For entire test parts, ΔT implies the complete duration of the test parts, while for individual slump events, ΔT is defined as the period since the previous slump event or the beginning of the test for the first slump event in a test. Slump events are identified using time stacks of the video data, see for example Figure 4.14. As slump events take place at varying cross-shore locations, ΔT is determined for nine different cross-shore transects separately. Additionally, not all test parts were entirely recorded by the cameras, resulting in gaps in the video datasets. For the first slump events following such a gap, ΔT was estimated as the period since the gap in the time series. It should therefore be kept in mind that a number of slump events have underestimated values for ΔT. These are indicated in red in Appendix D.

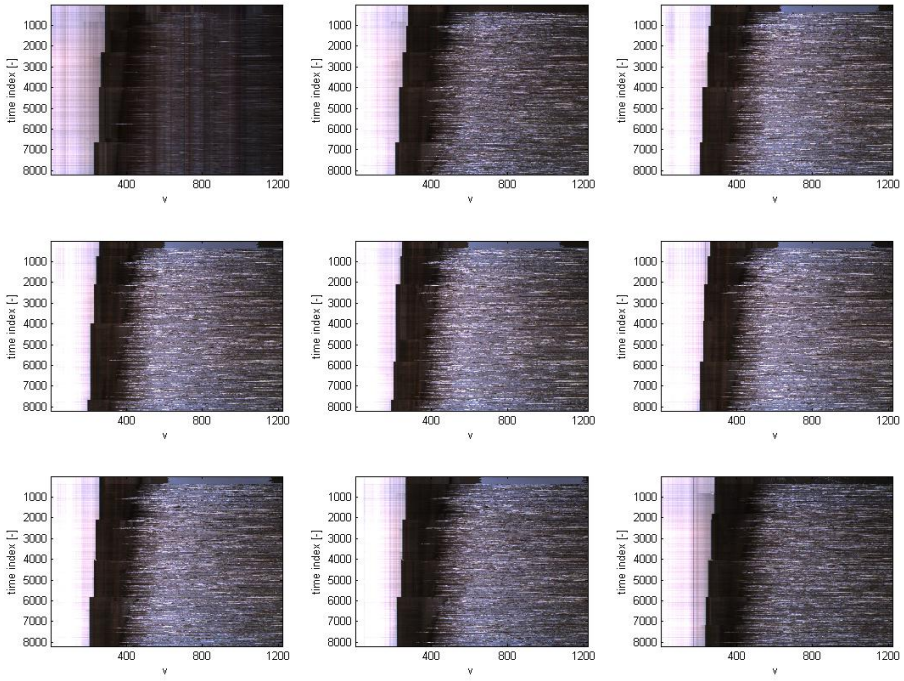

Figure 4.14 Time stacks for nine cross-flume transects in test DP01C, in which the slump events are visible as discontinuities in the location of the dune crest.

5 Results and discussion

The relation is studied between wave impact and sediment flux as defined in the previous chapter and derived from data of the Delta flume experiments. First, the results are examined for the time scale of entire test parts, followed by the results for individual slump events.

5.1 Entire test parts

Figure 5.1 shows sediment flux against wave impact during the entire test parts. The figure reveals coherence between the two, with a decline in both sediment flux as well as in wave impact with progress of the test. This decline is to be expected, as wave impact on the dune face and frequency of slump events decrease with the development of the dune and beach profile (see Section 3.4). The data points corresponding with test parts A however seem to show a different relation than the other data points.

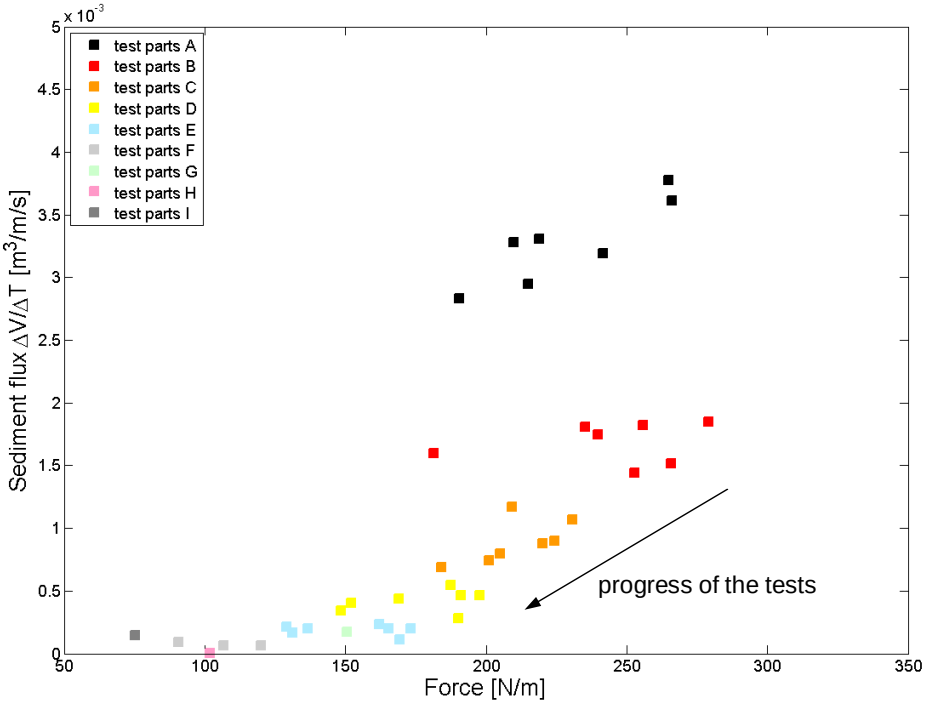

Figure 5.1 Erosion volumes against wave impact for entire test parts. The results for different test parts are plotted separately, showing that the erosion volumes decrease with progress of the test. Test parts A seem show another relation with respect to the other test parts.

The dissimilarity in the relation between data points A and data points B to I is probably related to the shape of the cross-shore profile which strongly determines the occurring dune erosion process. The profile change can be illustrated by the developments in time of two characteristic parts of the profile, i.e. the dune face and beach. These are derived from the test results as described in Section 3.4.

First of all, the progress of the toe level of the dune face is considered. The toe level is defined as the level of the lowest point of the dune face, being the point at the bottom of the dune face where the gradient of the profile slope is maximal. In the initial profile of all tests, the toe level is located below SWL. During test parts A the toe level increases rapidly. At the end of test parts A the toe level is above SWL. It remains above SWL throughout the rest of the test parts.

Additionally, the slope of the dune face steepens rapidly during test part A, while it remains nearly constant during the subsequent test parts. The slope of the beach close to the dune is steepened rapidly during the first part of test A, and significantly slower during the remaining test parts. The slope of the beach further from the dune however is steepened throughout the tests, approaching an equilibrium profile corresponding with the storm conditions.

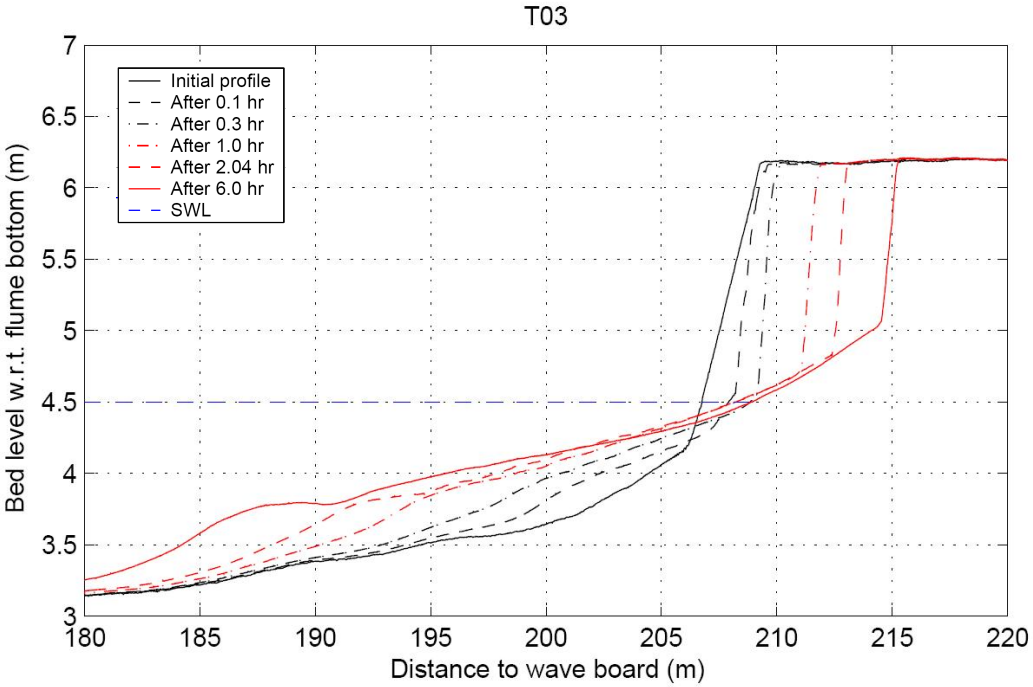

Figure 5.2 Development of average cross-shore profile for test T03, derived from the three in-situ measured profiles after each test part.

With this reshaping of the dune and beach profile, the process of dune erosion as a result of wave impact changes fundamentally. Initially, the dune toe level is below SWL and the slope of the dune face 1:1.5, implying that waves run up and down the dune face without directly impacting it. Apparently, steepening of the dune face is the dominant erosion mechanism during the first 0.1 hour of the tests, while slumping from the upper dune face is hardly or not taking place (see inventory of slump events in Appendix D and Figure 5.3). The dune crest remains at its initial location during this phase, while the waves scrape off sand from the dune face, steepening it rapidly. It appears that mainly dune erosion mechanism (c), sliding and flowing, occurs during the first 0.1 hours of the tests (see Section 2.2).

When the dune toe level is elevated above SWL, after approximately 0.1 hour, waves run up the beach before hitting the dune face. When waves run up and down the beach, the near-vertical dune face is periodically impacted by a travelling mass of water, eventually resulting in a slump event. In this situation, erosion mechanism (b): notching and slumping and erosion mechanism (c) sliding and flowing occur simultaneously (see Section 2.2).

After 0.1 hour of the test a fundamentally different dune face erosion process thus takes place than during the first minutes. As it appears in Figure 5.1, the erosion process during the first stage of the tests results in a significantly higher sediment flux than the process during the remaining time of the tests.

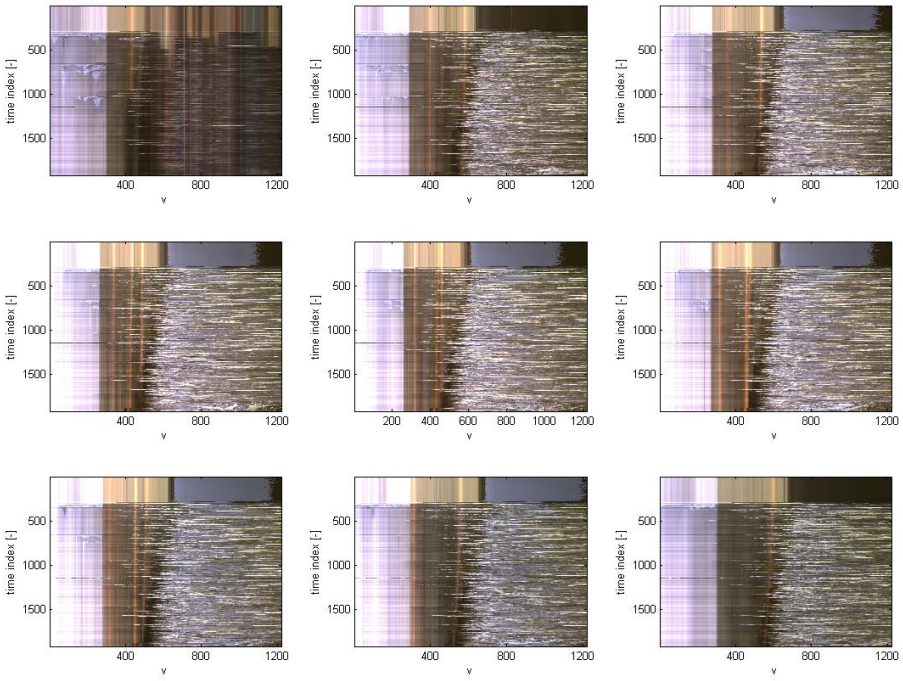

Figure 5.3 Time stacks for nine cross-flume transects in test DP01A. The dune crest remains on its initial location, while the slope of the dune face (the brownish part to the right of the dune crest) appears to retreat in time.

According to the results in Figure 5.1, the transition between the two erosion processes occurs in the dune erosion process after 0.1 hour of the tests. It is possible that the transitional phase ends slightly later than 0.1 hour after the start of the test, implying that the data points of test parts B (see Figure 5.1) are influenced by the transitional phase. In Figure 5.4, data points corresponding with test parts C to I are plotted. These data points clearly show coherence. Various functions can be fitted through the data points. The simplest function would be a linear polynomial, see Figure 5.4. This function intersects with the horizontal axis, implying a threshold wave impact above which erosion takes place. This seems logical for the case of the periodical primary erosion, where a slump event takes place after a period of wave impact. However, primary and secondary erosion occur simultaneously. A more complex relation is therefore expected which also accounts for the continuous secondary erosion, i.e. small erosion volumes as a result of single wave impacts.

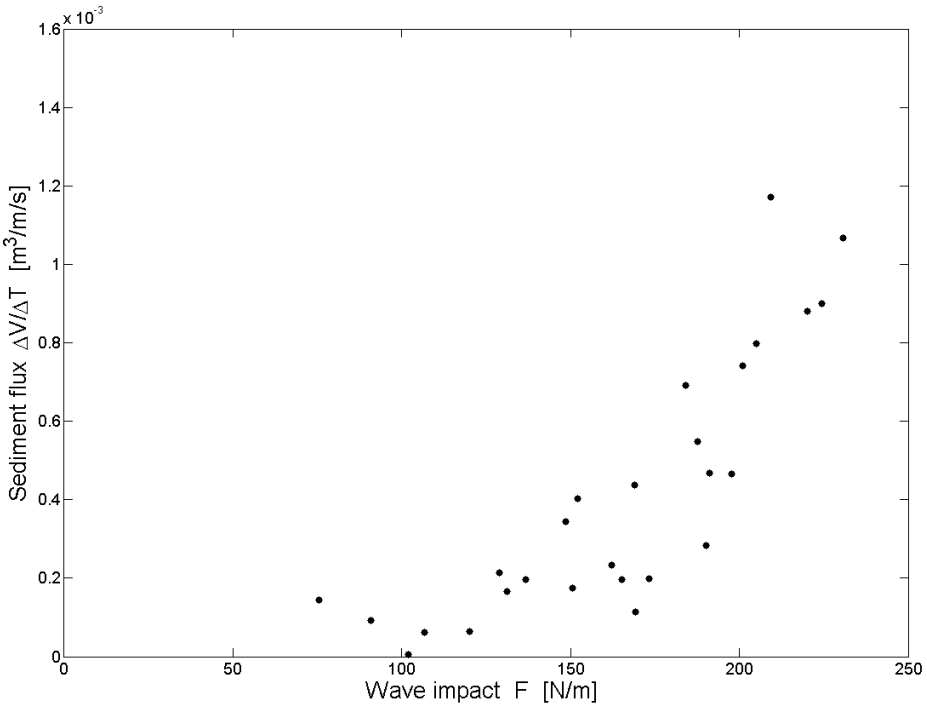

Figure 5.4 Results for data points corresponding with test parts C to I.

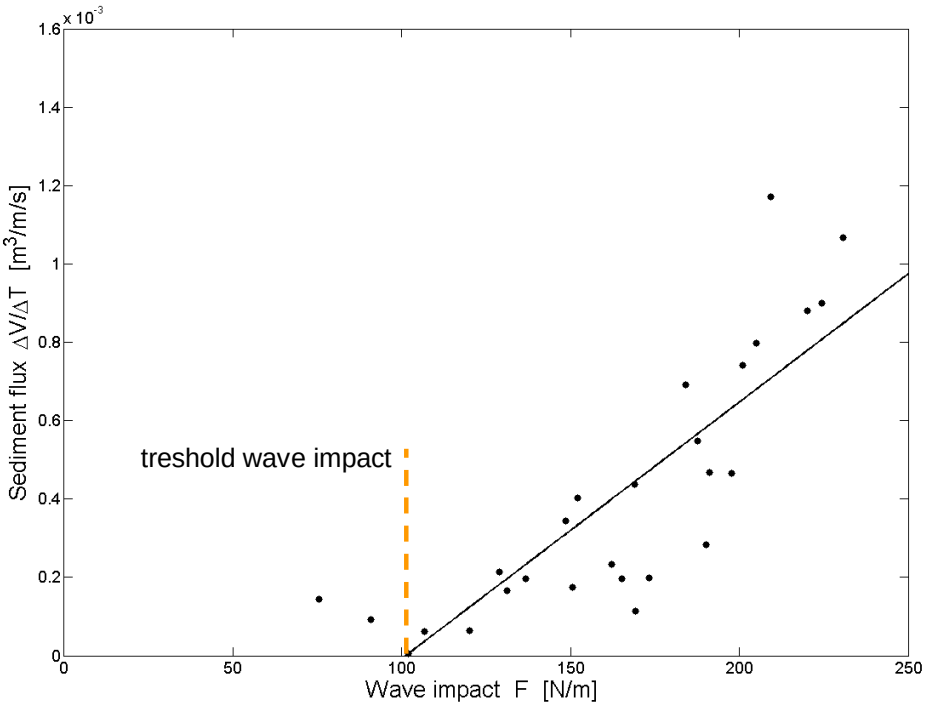

Figure 5.5 A linear polynomial fitted through the results for data points corresponding with test parts C to I, using a linear least square method with coefficients within 95% confidence bounds. The function intersects with the horizontal axis implying a threshold wave impact of slightly more than 100 N/m.

5.2 Individual slump events

In Figure 5.6 the results for wave impact and sediment flux are plotted for individual slump events together with the results for entire test parts. These data points agree reasonably with the data points for entire test parts, but do not show much coherence themselves. This is probably caused by a lot of scatter, which can be explained by possible uncertainties that are introduced when calculating volumes from video data:

- Uncertainty in the determination of period ΔT. As mentioned in Section 4.3.3, a large part of the data points has an underestimated value for ΔT. When the data points with inaccurate values for ΔT are left out, the results do still not show high coherence, see Figure 5.7.

- Uncertainty in calculating volumes from retreat areas. The relation between retreat area and volume appears to be linear, however quite some scatter occurs. An error is thus introduced when converting retreat areas into volumes using this relation.

- 3D-effects play a role when considering individual slump events. As mentioned in Section 3.4, dune crest retreat is uniform over the width of the flume averaged over a number of slump events. Dune erosion can therefore be considered as a 2D-process when studying a series of slump events. This is however not the case when considering single slump events. An error is thus introduced when considering the process as a 2D-process.

- Uncertainty in definition of camera geometries and camera and GCP positions (see Section 3.3.2). This error is however not likely to be of such order that resulting profiles and volumes cause the scatter in Figure 5.6. From visual observations of plots of 3D-profiles calculated, profiles appear to be very well reproduced and agree with in-situ measured profiles.

- Uncertainty in stereo processing of video data into 3D-profiles. When pixels are not accurately matched between two images, an error is generated in the (x,y,z)-coordinates for the corresponding point in space. To stereo match pixels, minimum contrast and distinct features are necessary. It is plausible that parts of the images lack these characteristics, resulting in errors in the calculated 3D-profile.

Uncertainties are thus probably generated on all of these levels, each causing part of the scatter. The accumulation of these errors might be the explanation for the considerable scatter in Figure 5.6 and Figure 5.7.

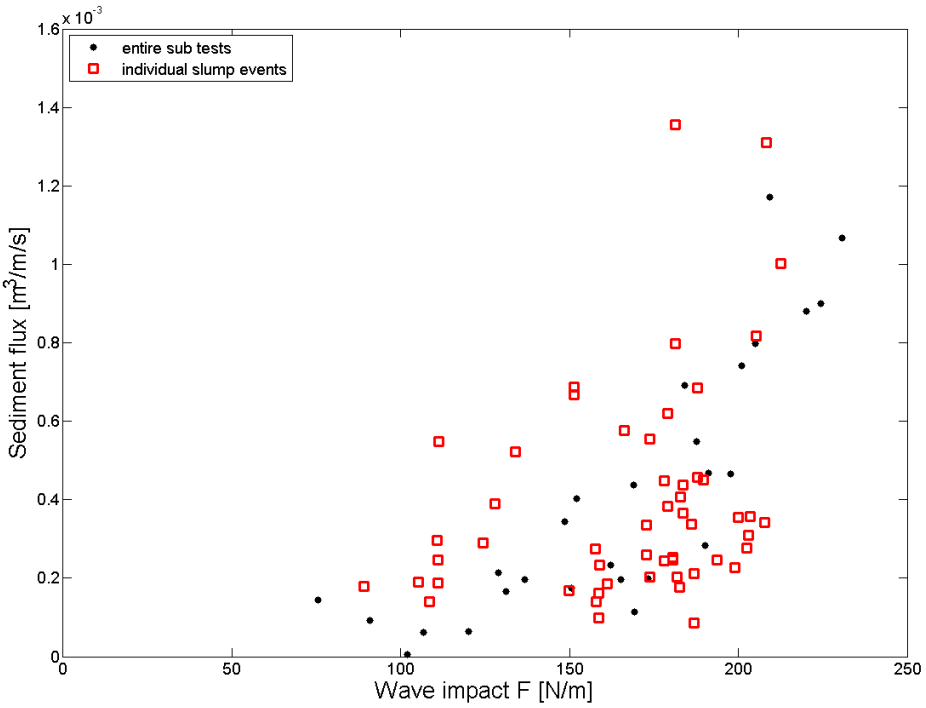

Figure 5.6 Results for individual slump events, plotted together with the results for entire test parts

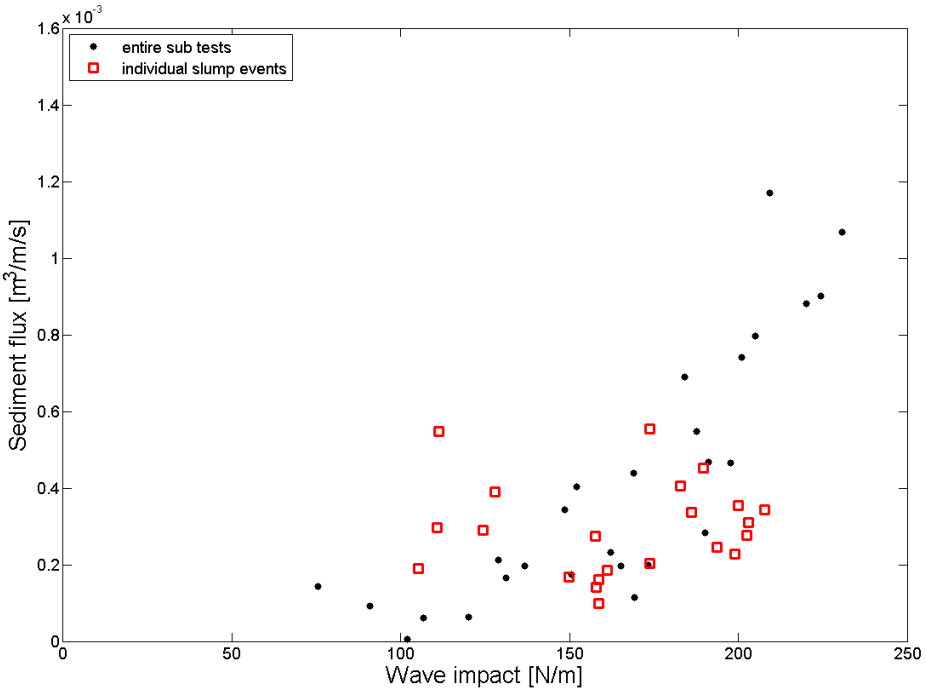

Figure 5.7 Results for individual slump events, plotted together with the results for entire test parts, leaving out the data points for which the period ΔT could not be determined accurately.

5.3 Comparison with the model by Fisher *et al.* (1986)

Fisher *et al.* (1986) found a linear relation between specific wave impacts and specific erosion volumes, see Section 4.2. The results of this research as presented in the previous paragraphs cannot as such be compared with the results of Fisher *et al.* (1986). First of all, sediment flux is examined in this research, while Fisher *et al.* (1986) studied erosion volumes. Additionally, the definition of wave impact diverts from the one by Fisher *et al.* (1986) such that the two are not comparable. It can however be concluded from the results of this research that a relation also exists between wave impact and sediment flux when taking into account the time scale of slump events.

For the combination of a wave-impact driven dune face erosion model with a process-based morphodynamic model for the nearshore, the model presented in this research is more practicable than the model proposed by Fisher *et al.* (1986). The exchange of wave impact and sediment flux between a nearshore model and the dune erosion model can be realised per time step, while the model by Fisher et al. (1986) exchanges information on the time scale of single waves.

6 Conclusions and recommendations

6.1 Conclusions

For this research data obtained during large-scale dune erosion experiments in the Delta flume of WL | Delft Hydraulics were used. During these experiments, two dune erosion mechanisms appeared to occur. On the one hand, when the dune face reaches a critical steepness, the dune face collapses and a volume of sand falls down on the beach. This periodical slumping is called primary erosion. On the other hand, each wave running up the dune face between the slump events erodes a layer off the dune face, steepening it continuously. This is called secondary erosion.

To study the relation between wave impact and sediment flux, wave impact was defined as the mean force of the waves on the dune face during a certain period of wave attack. Sediment flux is defined as the volume of sand eroded per unit of time, in which dune erosion volume is the total dune erosion volume, i.e. primary plus secondary erosion. This method does not distinguish between the two erosion mechanisms.

According to the results as presented in Chapter 5, there is a clear coherence between wave impact and sediment flux when the dune face experiences wave attack. Several possible functions can be fitted through the data points corresponding to the situation where the toe of the dune is above still water level and the dune face has a near-critical slope. This situation arises after a few minutes of the experiments. The data points for the situation at the start of the experiments, when the dune face is partly below SWL, also show strong coherence, but clearly according to a different relation. Apparently, wave impact causes a relatively high sediment flux in this start-up situation.

The difference in the relation between wave impact and sediment flux between the two situations is based on the occurring erosion process. At the start of the experiments, waves run up and down the mildly sloping dune face, steepening it rapidly. The erosion process is then the gradually sliding and flowing of sand from the dune face. Mainly secondary erosion takes place. When the dune face reaches certain steepness and is raised completely above SWL, waves have to run up the beach before hitting the near-vertical dune face. This different wave attack causes the periodical slumping. Primary and secondary erosion now occur simultaneously. This is a fundamentally different dune erosion process, resulting in a different relation between wave impact and sediment flux from the dune face.

6.2 Recommendations

Wave-impact driven dune face erosion model

- Study the relation between wave impact and sediment flux for primary and secondary erosion separately. As primary and secondary erosion cause respectively periodical and continuous sediment flux from the dune face, it is desirable to process them separately as input in a nearshore sediment transport model.

- Study the influence of other factors on dune erosion. It is plausible that factors like sediment characteristics, wave period, presence of vegetation and surf beat also have influence on the occurring sediment flux. When including these parameters in a model for sediment flux, dune erosion can be predicted more accurately.

Instrumentation for dune erosion research

- The use of the stereo video technique proves to be lucrative in dune erosion research. Individual slump events were calculated, which cannot be done with in-situ measurements. A recommendation for future use of the technique is first of all that light intensity on the beach and dune face should be monitored continuously to guarantee the possibility of properly stereo processing of the images. Moreover, gaps have to be avoided in the video data during future wave-impact driven dune erosion experiments, as the entire duration of the tests are relevant for the proper calculation of wave impact and sediment flux.

- Measurements of a pressure sensor and flow velocity sensor located approximately 10 m from the initial dune face were used to derive wave impact on the dune face. It is strongly recommended for future wave-impact driven dune face erosion research to obtain wave impact data at the location of the dune face, to be able to relate wave impact to dune erosion volumes more accurately. It would be interesting to study the possibility of using video images and stereo video calculations for this purpose.

7 References

AARNINKHOF, S.G.J. (2003), Nearshore Bathymetry derived from Video Imagery, PhD Thesis, Delft University of Technology

AARNINKHOF, S.G.J., I.L. TURNER, T.D.T. DRONKERS, M.CALJOUW, L.NIPIUS (2003), A video-based technique for mapping intertidal beach bathymetry, In: Coastal Engineering 49 (2003), p.275-289

BATTJES, Prof.dr.ir. J.A. (2002), Fluid Mechanics, lecture notes

BATTJES, Prof.dr.ir. J.A. (2001), Short Waves, lecture notes

BOS, C. (2006), Wave characteristics derived from video, MSc Thesis, 2006

COEVELD, E.M., J.H. DE VROEG (2005), Progress Report Dune Erosion Tests, H4357, December 2005

DOUCETTE, J.S., E.S. HARVEY, M.R. SHORTIS (2002), Stereo-video observation of nearshore bedforms on a low energy beach, In: Marine Geology 189 (2002), p. 289-305

FISHER, J.S., A. ASCE, M.F. OVERTON, Asooc. M. ASCE, T. CHISHOLM (1986), Field Measurements of Dune Erosion, In: Coastal Engineering-1986, p.1106-1114

GUZA, R.T., E.B. THORNTON (M.ASCE), R.A.HOLMAN (1984), Swash on Steep and Shallow Beaches, In: Coastal Engineering – 1984, p.708-723

HOLLAND, K.T., R.A. HOLMAN, T.C. LIPPMANN, J. STANLEY, N. PLANT (1997), Practical Use of Video Imagery in Nearshore Oceanographic Field Studies, In: IEEE journal of Oceanic Engineering, vol. 22, No. 1, p. 81-92

HOLLAND, K.T., R.A. HOLMAN (1997), Video Estimation of Foreshore Topography Using Trinocular Stereo, In: Journal of Coastal Research, vol. 13, No. 1, p.81-87

LARSON, M., L. ERIKSON, H. HANSON (2004), An Analytical model to predict dune erosion die to wave impact, In: Coastal Engineering 51 (2004), p. 675 - 696

NISHI, R., N.C. KRAUS (1996), Mechanism and calculation of sand dune erosion by storms, In: Coastal Engineering 1996, p.3034 - 3047

NOORLOOS, VAN J.C. (2003), Energy transfer between short wave groups and bound long waves on a plane slope, MSc Thesis, 2003

OVERTON, M.F., FISCHER, J.S. (1988), Simulation Modeling of Dune Erosion, In: Coastal Engineering – 1988, p. 1857 – 1867

OVERTON, M.F., J.S. FISCHER, K.N. HWANG (1994), Development of a Dune Erosion Model using SUPERTANK Data, In: Coastal Engineering – 1994. p.2488-2502

RENIERS, A.J.H.M., J.A. ROELVINK, E.B. THORNTON, Morphodynamic modeling of an embayed beach under wave group forcing, In: Journal of Geophysical Research, vol.109, C01030, 2004

RIJN, L.C. VAN (1993), Principles of Sediment Transport in Rivers, Estuaries and Coastal Seas, 1993

STEETZEL, H.J. (1993), Cross-shore transport during Storm Surges, PhD Thesis, Delft University of Technology, 1993

TILMANS, W.M.K (1981), Onderzoek naar duinafslag tijdens superstormvloed: toetsing van de resultaten van het twee-dimensionale modelonderzoek door middel van onderzoek in een drie-dimensionaal model, WL | delft hydraulics, 1981

TURNER, I.L., S.G.J. AARNINKHOF, R.A. HOLMAN (2006), Coastal Imaging Applications and Research in Australia, In: Journal of Coastal Research, vol. 22, No. 1, p. 37-48

VELLINGA, PIER (1986), Beach and Dune Erosion during Storm Surges, PhD Thesis, Delft University of Technology

WL | DELFT HYDRAULICS, i.c.w. TU DELFT, UNIVERSITY OF TWENTE, UTRECHT UNIVERSITY (2007), Report H4357, Measurement report large-scale model tests

A In-situ instruments

Photo A.1 Amphibious profile follower, here positioned on top of the dune

Photo A.2 Flow velocity meter EMS (above) and pressure sensor PS (below) attached to the flume wall

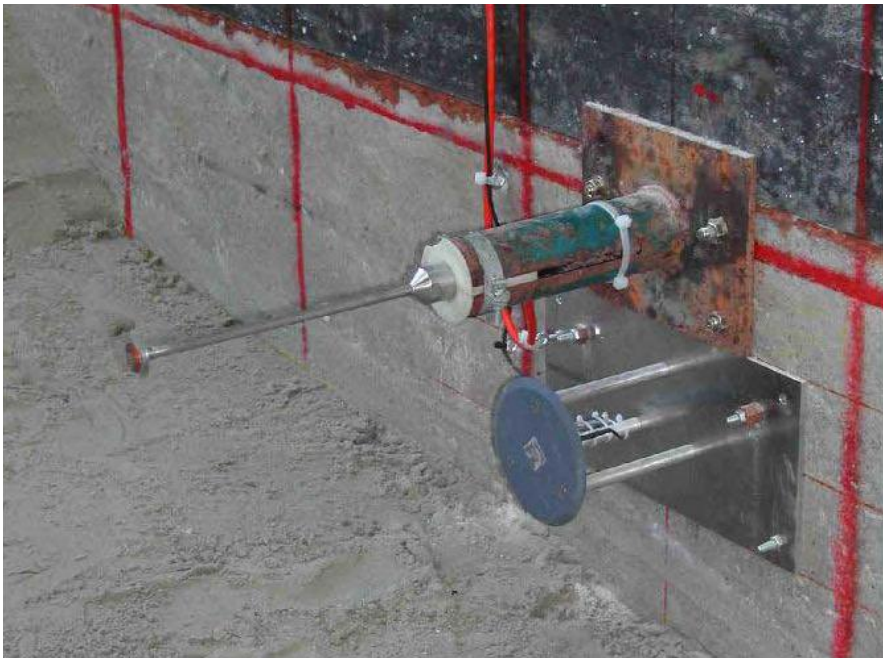

Photo A.3 Position of cameras (top) w.r.t. the Delta flume (below)

Photo A.4 One of the cameras fixed to the roof of the flume shed

B Test program

Test	Interval	Start [h]	End [h]	H_{m0} [m]	T_p [s]	$T_{m-1,0}$ [s]	s_p [-]	$s_{m-1,0}$ [-]
T01	A-E	0.0	6.0	1.5	4.9	4.45	0.040	0.049
T02	A-E	0.0	6.0	1.5	6.12	5.56	0.026	0.031
T03	A-E	0.0	6.0	1.5	7.35	6.68	0.018	0.022
T05	A-E	0.0	6.0	1.5	7.35	6.68	0.018	0.022
	F	6.0	7.0	0.8	7.35	6.68	0.018	0.022
T06	A-E	0.0	6.0	1.5	4.9	4.45	0.040	0.049
	F	6.0	6.5	1.5	4.9	4.45	0.040	0.049
	G	6.5	8.5	1.5	7.35	6.68	0.018	0.022
	H	8.5	9.5	0.5	7.35	6.68	0.006	0.007
	I	9.5	11.7	1.4	5.00	4.54	0.036	0.044
DP01	*A-E	0.0	6.0	1.5	6.12	3.91	0.026	0.063
	F	6.0	7.0	0.5	7.35	6.68	0.006	0.007

Table B.1 Test programme with hydraulic conditions near wave board ($T_{m-1,0} = T_p$ /1.1) *Double-peaked spectrum: $T_p = T_p(1)$ and $T_{m-1,0} \neq T_p$ /1.1

C Profile development

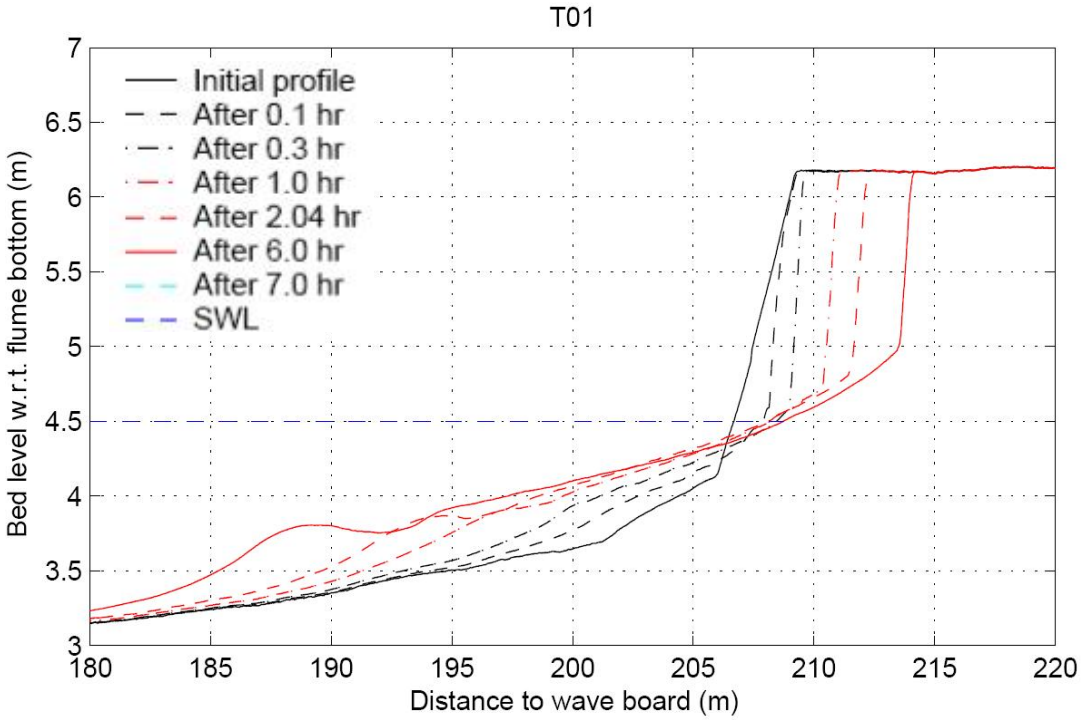

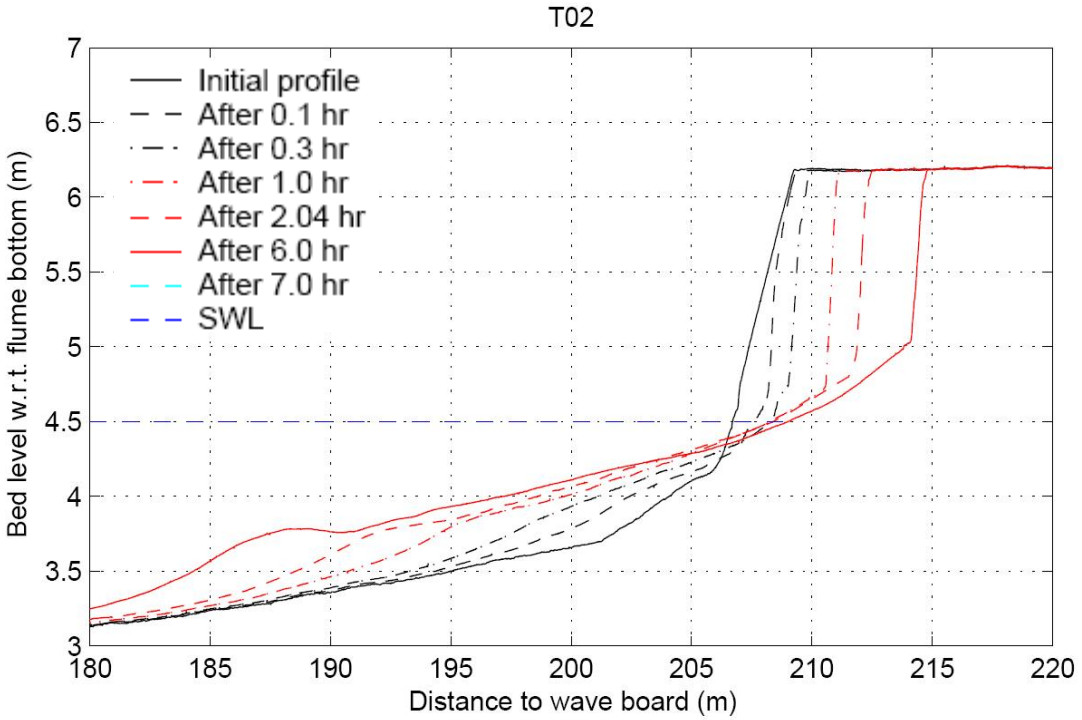

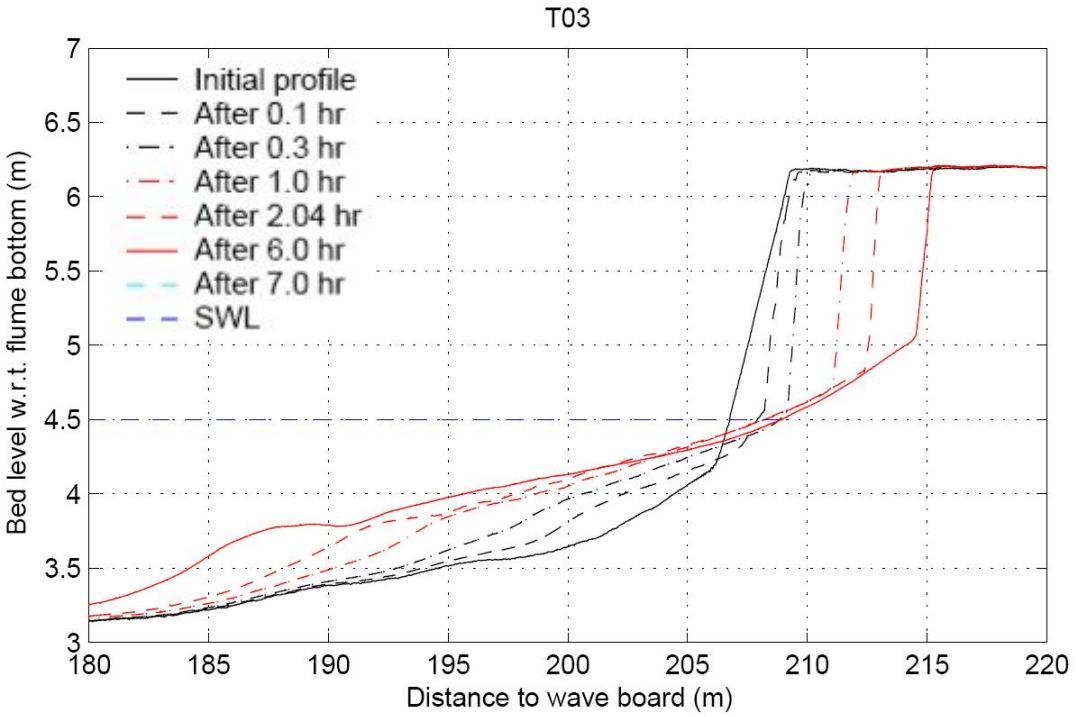
T03
Initial profile
After 0.1 hr
After 0.3 hr
After 1.0 hr
After 2.04 hr
After 6.0 hr
After 7.0 hr
SWL
Bed level w.r.t. flume bottom (m)
Distance to wave board (m)
7
6.5
6
5.5
5
4.5
4
3.5
3
180
185
190
195
200
205
210
215
220

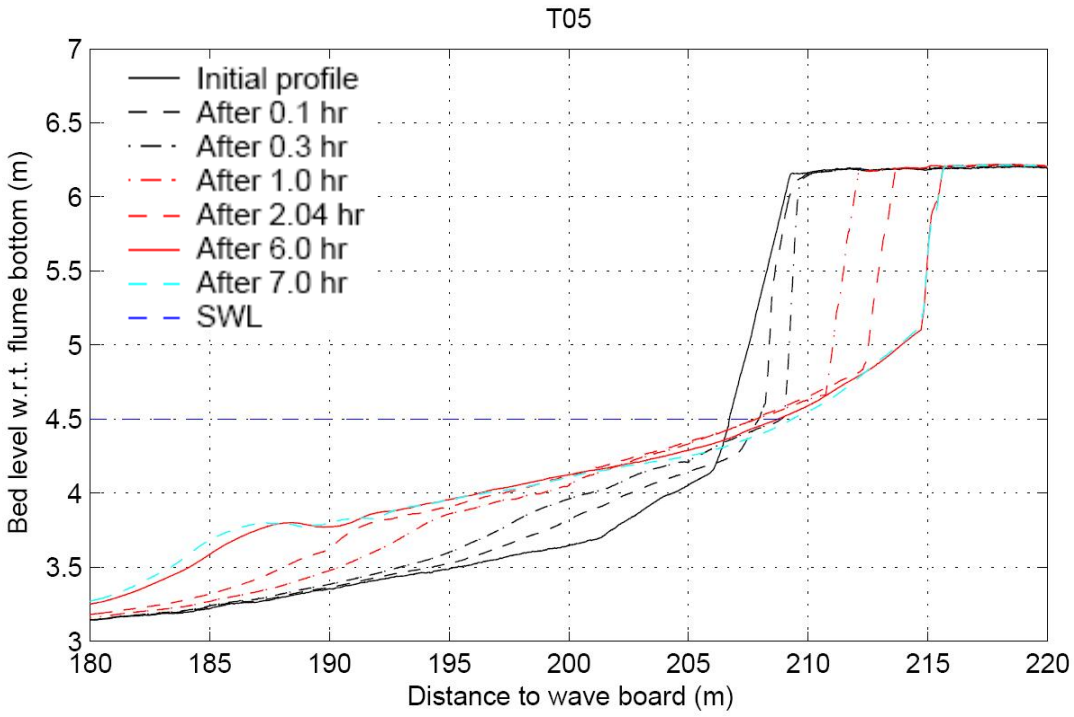
T05
Initial profile
After 0.1 hr
After 0.3 hr
After 1.0 hr
After 2.04 hr
After 6.0 hr
After 7.0 hr
SWL
Bed level w.r.t. flume bottom (m)
Distance to wave board (m)
7
6.5
6
5.5
5
4.5
4
3.5
3
180
185
190
195
200
205
210
215
220

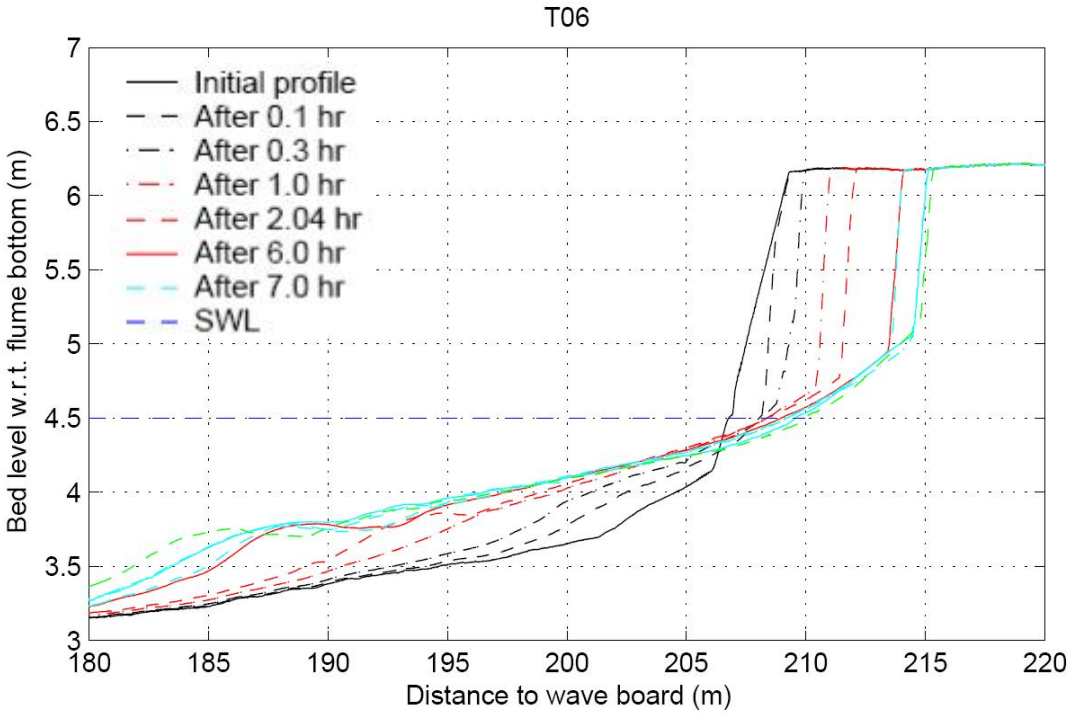
T06
Initial profile
After 0.1 hr
After 0.3 hr
After 1.0 hr
After 2.04 hr
After 6.0 hr
After 7.0 hr
SWL
Bed level w.r.t. flume bottom (m)
Distance to wave board (m)
7
6.5
6
5.5
5
4.5
4
3.5
3
180
185
190
195
200
205
210
215
220

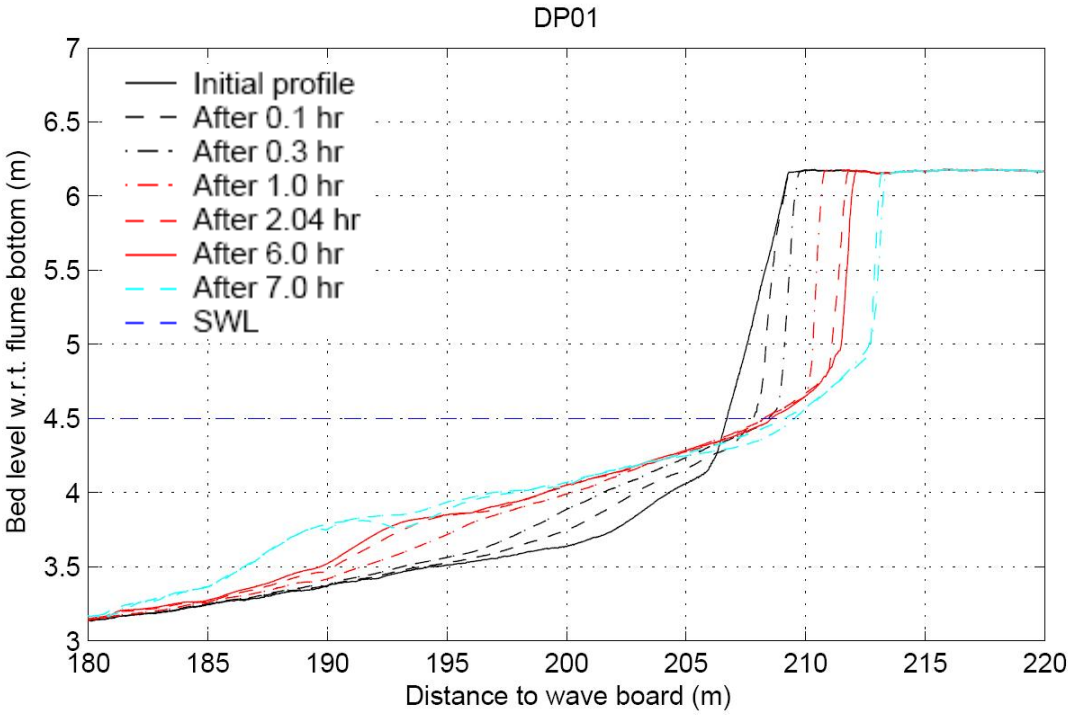
DP01
Initial profile
After 0.1 hr
After 0.3 hr
After 1.0 hr
After 2.04 hr
After 6.0 hr
After 7.0 hr
SWL
Bed level w.r.t. flume bottom (m)
Distance to wave board (m)
7
6.5
6
5.5
5
4.5
4
3.5
3
180
185
190
195
200
205
210
215
220

D Inventory of slump events

In the following tables, the slump events per transect are indicated with time indices. The upper number in the cell is the ΔT preceding the slump, the lower number is the exact time index for the occurrence of the slump. Left in the table, the average ΔT is given for the slump, as well as the start and end time index of the interval. Red numbers indicate that ΔT is not reliable due to lack of data.

T05D											
slump [-]	ΔT [s]	t_1 [s]	t_2 [s]	transects								
				1	2	3	4	5	6	7	8	9
1	786	0	786							786 786		
2	1184	0	1184									1184 1184
3	1182	196	1378				1378 1378	1378 1378	1378 1378	592 1378		
4	1485	0	1485	1485 1485	1485 1485							
t end video				2400	2400	2400	2400	2400	2400	2400	2400	2400

T05E												
slump [-]	ΔT [s]	t_1 [s]	t_2 [s]	transects								
				1	2	3	4	5	6	7	8	9
1	172	0	172	172 172	172 172	172 172						
2	677	0	677							677 677		
3	544	172	716	544 716	544 716							
4	823	0	823					823 823				
5	1435	86	1521			1349 1521	1521 1521					
6	1705	0	1705						1705 1705			
t end video				4062	4062	4062	4062	4062	4062	4062	4062	4062

T06C												
slump [-]	ΔT [s]	t_1 [s]	t_2 [s]	transects								
				1	2	3	4	5	6	7	8	9
1	379	0	379								379 379	379 379
2	661	0	661			661 661	661 661	661 661	661 661			
3	843	330	1173						512 1173	1173 1173		
t end video				2040	2040	2040	2040	2040	2040	2040	2040	2040

T06D												
slump [-]	ΔT [s]	t_1 [s]	t_2 [s]	transects								
				1	2	3	4	5	6	7	8	9
1	440	0	440						440 440	440 440	440 440	440 440
2	1292	0	1292	1291 1291	1291 1291	1292 1292	1293 1293					
3	1803	440	2243									1803 2243
t end video				2640	2640	2640	2640	2640	2640	2640	2640	2640

T06E												
slump [-]	ΔT [s]	t_1 [s]	t_2 [s]	transects								
				1	2	3	4	5	6	7	8	9
1	117	0	117						116 116	117 117		
2	1619	0	1619	1620 1620	1619 1619	1619 1619	1619 1619	1619 1619				
3	2149	39	2188							2071 2188	2188 2188	2188 2188
t end video				2139	2139	2139	2139	2139	2139	2139	2139	2139

T07B												
slump [-]	ΔT [s]	t_1 [s]	t_2 [s]	transects								
				1	2	3	4	5	6	7	8	9
1	1065	0	1065	1066 1066	1065 1065	1065 1065	1065 1065	1065 1065				
2	601	533	1134	68 1134								1134 1134
3	735	549	1284		221 1284					1284 1284	1284 1284	150 1284
4	467	982	1449					384 1449	1449 1449	167 1449	167 1449	167 1449
t end video				1734	1734	1734	1734	1734	1734	1734	1734	1734

T07C												
slump [-]	ΔT [s]	t_1 [s]	t_2 [s]	transects								
				1	2	3	4	5	6	7	8	9
1	1151	-412	739				1408 739	1024 739	1024 739			
2	1593	-558	1035		1483 1035	1704 1035						
3	2073	-284	1789									2073 1789
4	1507	573	2080				1340 2080	1341 2080	1342 2080	2364 2080	2363 2080	291 2080
5	1819	490	2309	2909 2309	1274 2309	1274 2309						
6	1757	2080	3836						1757 3836			
7	1721	2252	3973	1664 3973	1664 3973	1664 3973	1893 3973					
8	1953	2080	4033							1953 4033	1953 4033	1954 4033
9	2216	3604	5819					3739 5819	1982 5819	1786 5819	1786 5819	1786 5819
10	2663	3972	6635	2662 6635	2664 6635	2663 6635						
11	1333	5820	7152									1333 7152
12	2461	5203	7664				3692 7664	1846 7664	1846 7664			
t end video				8188	8188	8188	8188	8188	8188	8188	8188	8188

T07D											
slump [-]	ΔT [s]	t_1 [s]	t_2 [s]	transects								
				1	2	3	4	5	6	7	8	9
1	**2235**	-1552	683	2235 683	2235 683	2236 683						
2	**2117**	-985	1132				1656 1132	1656 1132	1656 1132	3502 1132		
3	**3212**	-758	2454							1322 2454	4824 2454	3490 2454
4	**3262**	908	4169		3486 4169	3486 4169	3037 4169	3037 4169				
	3727	1830	5557					2520 5557	4425 5557	4235 5557		
5	**4280**	2454	6734								4280 6734	4280 6734
6	**6094**	684	6777	6094 6777								
t end video				8186	8186	8186	8186	8186	8186	8186	8186	8186

T07F											
slump [-]	ΔT [s]	t_1 [s]	t_2 [s]	transects							
				1	2	3	4	5	6	7	8	9
1	**3390**	0	3390			3390 3390	3390 3390	3390 3390	3390 3390			
t end video				8189	8189	8189	8189	8189	8189	8189	8189	8189

E Erosion volumes and wave impact for entire test parts

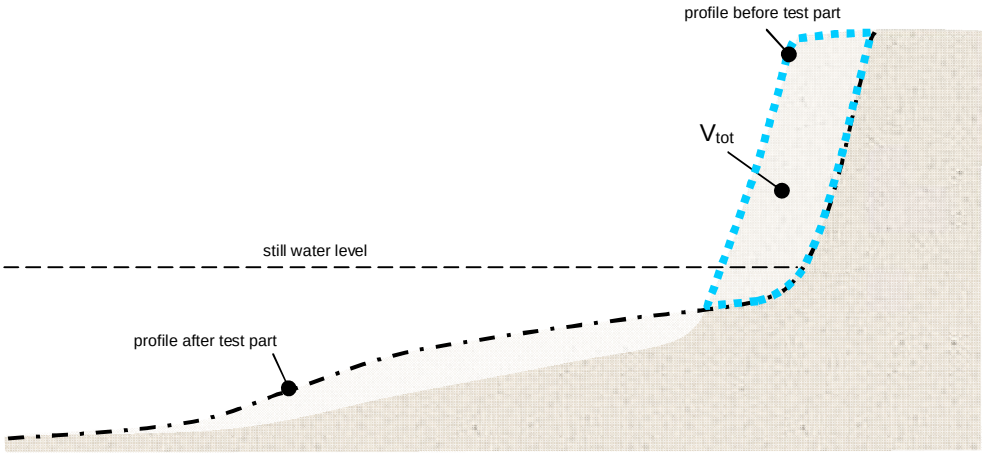

Figure E.1 Definition sketch of V_{tot}

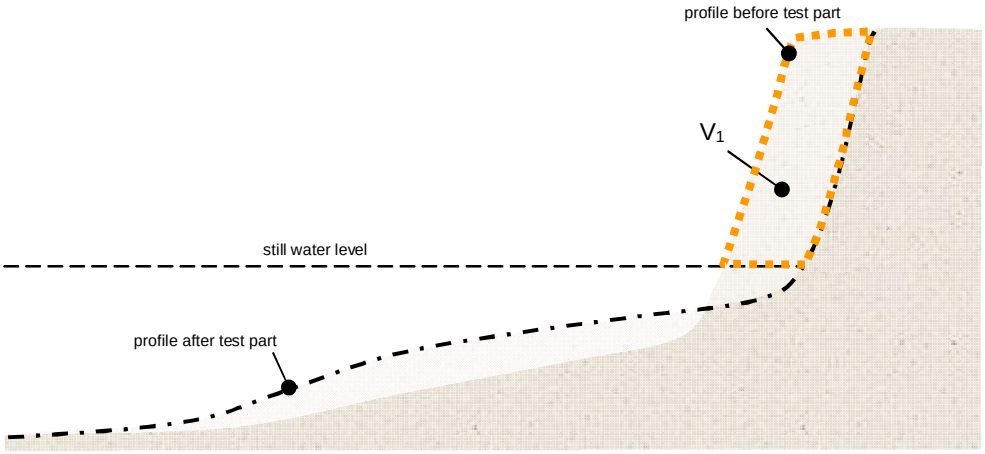

Figure E.2 Definition sketch of V_1 (WL | Delft Hydraulics, 2007)

Table E.1 Erosion volumes (WL | Delft Hydraulics, 2007) and corresponding wave impact for all test parts

Test nr	Test part	V_{tot} [m^3/m^1]	F [N/m]
T01	**A**	1.06	215.01
	B	1.26	239.66
	C	2.01	206.00
	D	1.63	169.08
	E	2.81	136.75

T02	**A**	1.15	241.45
	B	1.31	255.88
	C	2.22	220.11
	D	1.74	191.07
	E	3.33	162.08
T03	**A**	1.36	265.01
	B	1.33	279.05
	C	2.69	230.68
	D	1.79	197.61
	E	2.84	173.16
T05	**A**	1.30	266.06
	B	1.04	252.91
	C	2.95	209.30
	D	2.04	187.57
	E	2.81	165.27
	F	0.24	120.03
T06	**A**	1.18	209.76
	B	1.30	235.27
	C	1.87	201.05
	D	1.50	152.07
	E	2.93	129.03
	F	0.11	106.62
	G	1.26	150.61
	H	0.05	101.98
	I	0.47	75.37
DP01	**A**	1.02	190.58
	B	1.15	181.52
	C	1.74	184.17
	D	1.28	148.44
	E	0.51	131.12
	F	1.85	90.81

F Erosion volumes and wave impact for individual slump events

Table F.1 Primary erosion volumes and preceding wave impact for all slump events in the tests of the Delta flume experiments, derived directly from stereo video calculations (V_V) and from retreat areas (V_A)

Test nr	slump nr	Erosion volume V_V [m^3]	Erosion volume V_A [m^3]	Retreat Area A [m^2]	Period ΔT [ ]	Force F [N/m]
T05D	1	0.9756	0.6018	0.0702	393.00	179.01
	2	0.582	0.6012	0.0279	592.00	180.68
	3	0.792	0.6133	0.8767	591.00	172.77
	4	--	0.6040	0.2256	742.50	181.73
T05E	1	0.5646	0.6050	0.2959	86.00	209.85
	2	0.3308	0.6069	0.4288	338.50	178.17
	3	0.2215	0.6042	0.2346	272.00	173.73
	4	0.7183	0.6039	0.2154	411.50	183.68
	5	0.2433	0.6072	0.4470	717.50	186.95
	6	--	0.6031	0.1572	852.50	182.65
T06C	1	10.277	0.6045	0.2559	189.50	181.28
	2	0.9064	0.6049	0.2854	330.50	187.86
	3	--	0.6036	0.1962	421.50	203.62
T06D	1	0.5875	0.6056	0.3343	220.00	151.36
	2	--	0.6058	0.3499	646.00	159.00
	3	--	0.6058	0.3463	901.50	149.81
T06E	1	0.1222	0.6032	0.1650	58.50	134.02
	2	0.7956	0.6058	0.3521	809.50	111.07
	3	--	0.6049	0.2878	1074.50	108.58
DP01B	1	--	0.6026	0.1266	261.50	166.31
	2	--	0.6022	0.0949	150.25	212.59
	3	--	0.6013	0.0357	183.75	205.34
	4	--	0.6120	0.7877	116.75	208.36

Test nr	slump nr	Erosion volume V_V [m^3]	Erosion volume V_A [m^3]	Retreat Area A [m^2]	Period ΔT [ ]	Force F [N/m]
DP01C	1	--	0.6059	0.3598	276.25	111.28
	2	--	0.6039	0.2170	386.75	127.99
	3	--	0.6013	0.0348	506.75	110.66
	4	--	0.6125	0.8229	376.75	182.73
	5	--	0.6125	0.8229	454.75	186.02
	6	--	0.6016	0.0519	439.00	207.73
	7	--	0.6096	0.6162	430.25	199.90
	8	--	0.6041	0.2284	488.25	203.03
	9	--	0.6114	0.7450	553.75	202.45
	10	--	0.6056	0.3374	665.75	198.95
	11	--	0.6010	0.0120	333.00	189.55
	12	--	0.6058	0.3471	615.25	193.79
DP01D	1	--	0.6016	0.0557	548.75	157.62
	2	--	0.6018	0.0698	519.25	124.27
	3	--	0.6008	-	793.00	105.20
	4	--	0.6072	0.4448	815.25	161.27
	5	--	0.6040	0.2259	931.75	158.55
	6	--	0.6017	0.0630	1070.00	157.77
	7	--	0.6010	0.0138	1523.25	158.59
DP01F	1	--	0.6058	0.3503	847.50	89.00

G Development of slump interval in time

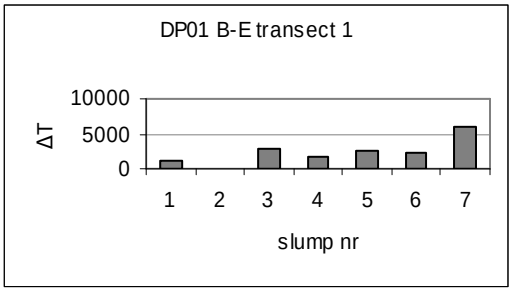

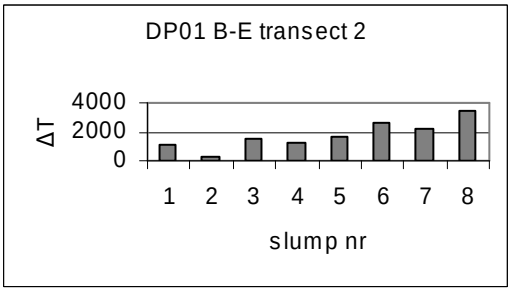

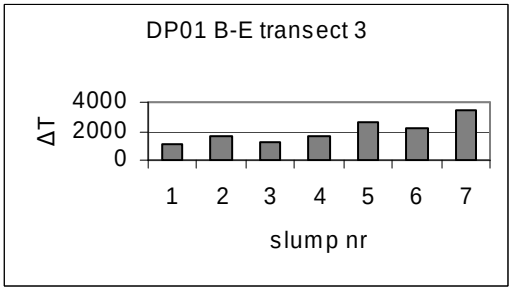

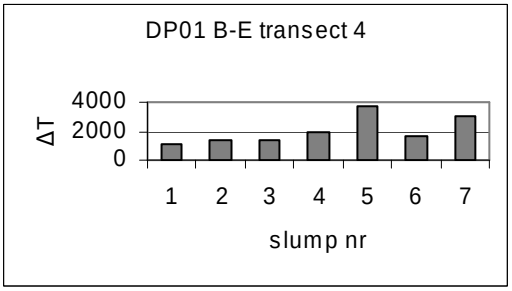

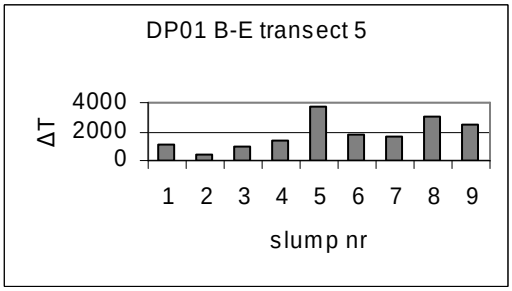

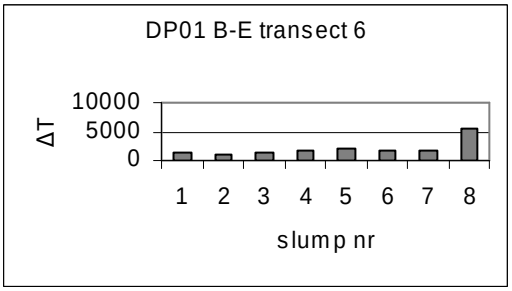

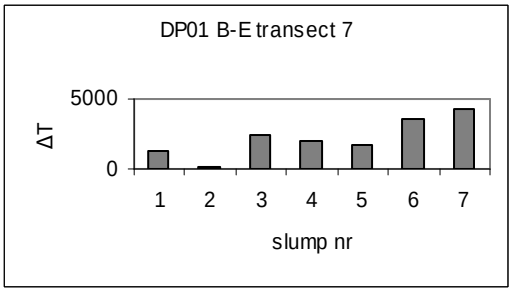

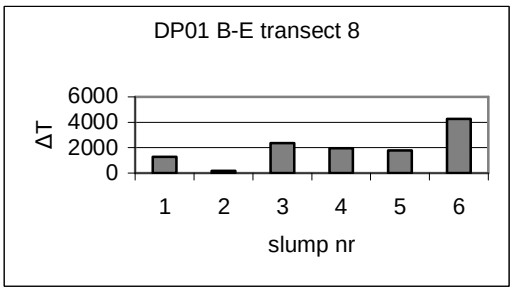

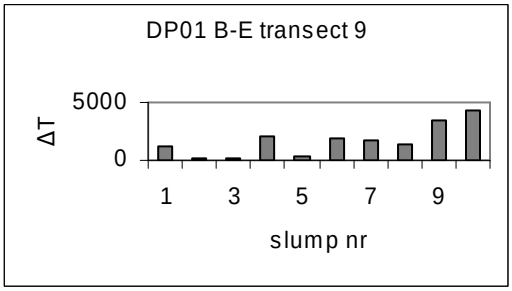

H Development of individual slump erosion volume in time